

Article

In Vitro Experimental Observations on Fungal Colonization, Metallophagus Behavior, Tunneling, Bioleaching and Bioweathering of Multiple Mineral Substrates

Kamal Kolo ^{1,*}  and Alain Pr at ² 

¹ Department of Biogeosciences, Scientific Research Center (SRC), Soran University, Soran 30802, Kurdistan Region, Iraq

² Research Group–Biogeochemistry & Modeling of the Earth System, Free University of Brussels (ULB), B-1050 Brussels, Belgium

* Correspondence: kamal.kolo@soran.edu.iq

Abstract: This study reports on experimental observations during fungi–mineral substrate interactions. Selected mineral substrates of biotite, muscovite, bauxite, chromite, galena, malachite, manganite, and plagioclase were exposed in vitro to free fungal growth under open conditions. The interaction produced strong biochemical and biomechanical alterations to the mineral substrates. Specifically, reported here is a three-dimensional thigmotropic colonization pattern of the mineral surfaces that suggested a possible pattern of fungal metallophagus behavior. Authigenic secondary mineral biomineralization occurred: Ca- and Mg-Oxalates such as weddellite: $\text{CaC}_2\text{O}_4 \cdot 2\text{H}_2\text{O}$, whewellite: $\text{CaC}_2\text{O}_4 \cdot \text{H}_2\text{O}$, and glushinskite: $\text{MgC}_2\text{O}_4 \cdot 2\text{H}_2\text{O}$; struvite: $(\text{NH}_4) \text{MgPO}_4 \cdot 6\text{H}_2\text{O}$; gibbsite: $\text{Al}(\text{OH})_3$; and gypsum: $\text{CaSO}_4 \cdot 2\text{H}_2\text{O}$. The bioleached elements included Fe, Pb, S, Cu, and Al, which formed single crystals or aggregates, amorphous layers, amorphous aggregates, and linear forms influenced by the fungal filaments. The fungi bioleached Fe and Al from bauxite and Mn from manganite and deposited the metals as separate mineral species. Gypsum was deposited during the interaction with the manganite substrate, indicating a source of Ca and S either within manganite impurities or within the fungal growth environment. Other biochemical and biomechanical features such as tunneling, strong pitting, exfoliation, dissolution, perforations, and fragmentation of the mineral surfaces were also produced. The results of this study, besides emphasizing the role of fungi in bioweathering and mineral alteration, also show that, to produce these alterations, fungi employ a 3D fungal colonization pattern of mineral surfaces guided by thigmotropic and possible metallophagus behavior.

Keywords: fungi; biomineralization; bioweathering; 3D colonization; metallophagus behavior; tunneling



Citation: Kolo, K.; Pr at, A. In Vitro Experimental Observations on Fungal Colonization, Metallophagus Behavior, Tunneling, Bioleaching and Bioweathering of Multiple Mineral Substrates. *Minerals* **2023**, *13*, 1540. <https://doi.org/10.3390/min13121540>

Academic Editors: Anna Panyushkina and Maxim Muravyov

Received: 20 October 2023

Revised: 6 December 2023

Accepted: 7 December 2023

Published: 12 December 2023



Copyright:   2023 by the authors. Licensee MDPI, Basel, Switzerland. This article is an open access article distributed under the terms and conditions of the Creative Commons Attribution (CC BY) license (<https://creativecommons.org/licenses/by/4.0/>).

1. Introduction

Fungi are often involved in the weathering of rock surfaces through both biomechanical and biochemical processes [1–5]. The weathering occurs as the fungi colonize rock surfaces, and their filaments (known as hyphae) exploit preexisting cracks, cleavages, and grain boundaries to gain access to new mineral resources. The depth and extension of the fungal attack on the mineral substrate, although controlled by various factors (fungi type, oxygen and nutrient availability, porosity, mineral composition, temperature, and light), is on the order of a few millimeters for lichenous fungi interacting with carbonate or granite rocks [6] to several meters in soil mycorrhizal fungi [7,8]. Fungal weathering occurs in both subaerial and aquatic environments [2,9], and their activity is directly relevant for the formation of soils and the breakdown of sedimentary organic matter. They are also destructive in the sense that they have been associated with the biodeterioration and degradation of cultural heritage monuments and edifices by causing pitting, exfoliation, and discoloration [10–12]. Fungi have been significant contributors to the cycling of elements

since their emergence on Earth approximately 1.5 billion years ago and their colonization of land around 650 million years ago [13–15]. Elements such as C, Ca, Mg, S, P, Fe, Mn, Al, Cu, and Cd are known to be mobilized or immobilized by fungi from natural mineral and rock substrates [16,17]. Biomechanical weathering effects are directly caused by the invasive growth and penetration of fungal hyphae into the rock substratum [2,3,10]. In doing so, they cause simple surface roughing by etching and pitting to extensive physical disintegration of the minerals that includes grain detachment and exfoliation [5,10]. Fungal appressoria also produce sufficiently high osmotic pressure to dislodge mineral grains [2,10]. In addition, many bacteria that grow alongside the fungi (i.e., as lichens) produce extracellular polymeric substances (EPSs) that enshroud all exposed mineral surfaces and, in doing so, help retain water to promote mineral fracturing, and it increases the residence time for water to drive hydrolysis reactions. Fungal biomechanical forces do not seem to play a major role in mineral alteration but rather facilitate the biochemical dissolution by rock disintegration, thus increasing the surface area exposed to organic acids.

The physical process works in tandem with the chemical dissolution of the minerals by organic acids (oxalic, citric, and malate) produced by the fungi. The acids dissolve minerals by two means: first, they produce protons that react with the ligands on the mineral surface, causing a weakening of the metal–oxygen bonds, and secondly, the organic anions react with metal cations at the mineral surface or in solution, thereby lowering the mineral’s saturation state (see [16,17] for details). These strong chelators and metal-binding acids [17] form complexes with various metals dissolved from the mineral substrata—Ca, Mg, Mn, Zn, Cu, Al, and Fe—in a process of metal mobilization and immobilization that ultimately facilitates the precipitation of new mineral phases [17,18]. The minerals formed by this process are mainly Ca- and Mg-oxalates (whewellite: $\text{CaC}_2\text{O}_4 \cdot \text{H}_2\text{O}$, weddellite: $\text{CaC}_2\text{O}_4 \cdot 2\text{H}_2\text{O}$, and glushinskite: $\text{MgC}_2\text{O}_4 \cdot 2\text{H}_2\text{O}$); carbonates (calcite: CaCO_3 and dolomite: CaMgCO_3); and struvite ($(\text{NH}_4) \text{MgPO}_4 \cdot 6\text{H}_2\text{O}$), although a wider variety of newly formed minerals have been shown to precipitate in response to a substrate’s specific mineralogy [1,2,5,8,19–21]. One such example is the feature known as desert varnish, an enigmatic iron- and manganese-rich crust that forms in subaerial environments by biomineralization, dissolution, metal transport, and transformation of the local rock substrata [1,5,17,18,22–25]. At other times, fungal metabolic products (organic acids) contribute less to mineral authigenesis than to the development of diagenetic “mycogenic fabrics” [1], such as crystal etching, grooves, borings, and “tunneling” by fungal hyphae [3,10]. In combination, the weathering of rocks and minerals by fungi significantly influences the biogeochemical cycle of organic or inorganic materials and plays a fundamental role in soil and sediment formation.

The fungal–mineral interactions extend to issues that impact the human environmental habitat, such as soil health in terms of quality and fertility [26]. Nutrients cycle through the decomposition of organic and inorganic materials, eventually maintaining a balanced ecosystem. The symbiotic relationship of mycorrhizal fungi is crucial for the growth of plants and crops, facilitating the breakdown of soil minerals and releasing important elements for plant growth, such as N, P, Ca, Fe, and S.

Despite an abundance of literature pertaining to fungally induced weathering, there is little information on the specific fungi–mineral interactions and how these microbes actually initiate the interaction and weathering process, especially on a micron scale. Accordingly, in this study, we investigate through experimental observational study using SEM and EDX imaging and mapping to record the *in vitro* specific patterns of fungi–mineral surface interactions in response to mineral chemistry, topography, and geometry and their associated bio-diagenetic products and focus on their modes of colonization, degradation and bioleaching. The studied colonization patterns suggest that certain fungi are capable of recognizing mineral geometry and topography on a micron scale and react to it in terms of growth directionality and colonization patterns, which also reveal, maybe for the first time, a possible metalophagus behavior by fungi against solid minerals. Additionally, it shows direct evidence of a thigmotropic sensing

of mineral substrate surfaces, which very much mimics how fungi naturally interact with mineral surfaces under natural conditions.

2. Experimental

2.1. Materials and Methods

Sample Description and Preparation

Natural samples of bauxite (diaspore (AlOOH)) and minerals muscovite ($\text{KAl}_2(\text{AlSi}_3\text{O}_{10})(\text{F,OH})_2$), biotite ($\text{K}(\text{Fe,Mg})_3\text{AlSi}_3\text{O}_{10}(\text{F,OH})_2$), galena (PbS), malachite ($\text{CuCO}_3 \cdot \text{Cu}(\text{OH})_2$), manganite $\text{MnO}(\text{OH})$, chromite ($\text{Fe,MgCr}_2\text{O}_4$), and plagioclase ($\text{Ca/Na-AlSi}_3\text{O}_8$) were selected from the mineralogical depository of the Department of Geology/Vrije Universiteit Brussel and examined for identity by a Siemens D500 X-ray diffraction (XRD), Siemens–Brussels, Belgium at the Department of Industrial Chemistry, Université Libre de Bruxelles, Brussels. A few of the hard samples (bauxite and malachite) were machine-cut and surface-smoothed into $4 \times 2 \times 1$ cm slab duplicates; galena, manganite, chromite, and plagioclase were used as chip fragments, while the muscovite and biotite samples were peeled and cut with metal scissors into $4.0 \times 2.0 \times 0.2$ cm and $4.0 \times 1.0 \times 0.2$ cm sections. All samples were thoroughly washed with distilled water and oven-dried at 40°C for 24 h before the experiments were started. For vertical mineral exposure, muscovite and biotite laminas were vertically and, in parallels of two-s or three-s, drop-glued onto glass slide surfaces at a minimum of 2.0 cm apart. For horizontal exposure, the tips of 2–3 muscovite and biotite laminas were horizontally glued to two parallel glass slides in a bridging form, directly laid at length on a glass slide, or glued on one end to a glass slide and left hanging free in the Petri dish. All other minerals used in this experiment, as slabs or chip fragments, were spread on glass slides covered with a thin film of commercial epoxy glue. All the experimental slides were elevated from the Petri dish base by laying them over 2–3 empty glass slides. At the end of the 12-week experiment, the rock and mineral slabs, chips, and peels were examined using light microscopy and scanning electron microscope (SEM) to observe their original settings.

2.2. Experimental

The mineral samples were separately placed in Petri dishes (90 mm in diameter) containing 20 mL of PDA (potato dextrose agar) and 20 g of untreated and freshly crushed almonds. This vegetable mixture has been previously shown to produce a dense growth of fungal mycelia and sporulation. Sterilization was not carried out, because the specimens were left exposed to free air circulation, variable light, and laboratory temperatures of $20\text{--}25^\circ\text{C}$. The growth medium surrounded the glass slides with mineral slabs, chips, and peels but did not touch their surfaces. Occasionally, the samples were sprayed with deionized water when the moisture content in the Petri dishes was low. Throughout the experiment, the samples were kept stationary, even when sampled for analysis. Fungal growth on the growth media was expected to occur naturally from airborne fungal spores. Observations were recorded every 24 h. The extracellular polymeric substance (EPS) layer that formed on the mineral substrata was examined under an optical microscope for biomineralization products. Slides for microscopic analysis were prepared without mounting material, cover glass, or staining to ensure an in situ image of the fungal–mineral interaction. The mineral slabs, as a whole, were subjected at the end of the experiment to SEM and EDX analyses of the mineral phases associated with the fungal mass.

This methodology that involves the cultivation of fungi in vitro under open conditions and allows them to interact with rock and mineral substrates has been refined over several years and aims to replicate natural conditions where rocks, sediments, and minerals are exposed to fungal and bacterial activity. The interactions between the fungi and the substrates are monitored over time, and the results are documented using scanning electron microscopy (SEM), energy-dispersive X-ray spectroscopy (EDX), Raman spectroscopy, and X-ray fluorescence (XRF). The observations made by the authors are found to be consistent with natural occurrences of fungal–mineral interactions, indicating the effectiveness of

the applied methodology; at the same time, changes in temperatures, humidity, seasonal changes, and, above all, time under a natural environment are all factors that point out the possible uncertainties in the lab work compared to nature.

Furthermore, the potential presence of impurities of other elements within the primary chemistry of the mineral substrates was taken into consideration, since their presence could add more outcomes to fungal interactions. Also, the organic growth media utilized could also introduce additional elements into the interaction process. These possibilities introduce an additional level of complexity to the primary fungal–mineral interaction. This complexity, when present, should be discussed within the broader context of the intricate interactions of fungi with rocks and minerals in nature, encompassing a diverse array of minerals, rock types, and elements. A notable illustration of this complexity is the symbiotic partnership between fungi and algae in lichens, which colonize various substrates in nature: a diverse array of rock types and minerals, leading to the production of a variety of biominerals that reflect the substrate’s chemistry.

2.3. Instrumentation

FE-SEM. High-resolution imaging (1.2–3.0 nm at 15 and 1 kV, respectively) was obtained with field emission scanning electron microscope (FE-SEM) JEOL JSM-7000 (Tokyo, Japan). The samples were sputter-coated with gold palladium and mounted on metal stubs.

SEM-EDX. The data pertinent to authigenic mineral morphology, distribution, chemistry, and the relationship of the fungal mass and EPS layer were acquired using scanning electron microscope (SEM) JEOL- JSM-6400 (Tokyo, Japan) at 20 kV and a working distance of 39 mm; the instrument was equipped with an energy-dispersive X-ray (EDX) (Thermo-Noran Pioneer with Si–Li detector, resolution 143eV cooled with liquid nitrogen, Waltham, MA, USA). The spectral treatment was performed with Sun Microsystems, Inc. Voyager III (UNIX Solaris operating system) and EDX software: NSS3 (Noran System Six, version 3, USA). Sample coating was done with an EMITECH Carbon evaporator K450 for carbon coating. The images and analyses were acquired in the normal and backscattered modes.

3. Results

3.1. Fungal Growth Patterns

3.1.1. Timing of Colonization

After 48 h, fine (5–10 μm) whitish and translucent fungal hyphae were observed on the solid parts of the growth media in all Petri dishes. By the fourth day, the fungal hyphae filled the entire Petri dish spaces and gradually displayed a darker color. Extensive sporulation started within the first week. The growing fungi formed a thick layer (3–4 mm) of mucilaginous material and fungal biomass that engulfed all mineral surfaces. It should be noted that the hyphae appeared to be well embedded onto the mineral surfaces and covered not only the smoother and planar surfaces but even three-dimensionally followed the rugged morphology of the substrata. This is a common observation for all minerals, irrespective of their mineralogy.

The fungi developed attachment rhizoids on the mineral surfaces and within the EPS. On the 10th day of the experiment, biomineralization on the fungal hyphae was microscopically observed on all mineral substrata as the fungal filaments began to display crystals directly attached to the hyphae together with authigenic minerals formed on the original mineral surfaces. The newly formed minerals decreased in abundance upward along the fungal hyphae. The lower parts of the hyphae attaching to the substrate and passing through the EPS showed a higher concentration of newly formed authigenic “biominerals”. In contrast, those parts of the filaments not attached to mineral surfaces did not display biominerals.

The strains of the growing fungi (Table 1) were isolated on contact plates filled with a malt chloramphenicol medium and incubated at 25 °C. After growth, the isolates were inoculated and identified on malt extract agar (MEA).

Table 1. The fungal strains isolated from the experimental mineral surfaces.

Mineral Sample	Fungal Strains	
Manganite	<i>Rhizopus oryzae</i>	
Muscovite/Biotite	<i>Rhizopus oryzae</i>	
Bauxite	<i>Rhizopus oryzae</i>	
Malachite	<i>Rhizopus oryzae</i>	<i>Aspergillus flavus</i>
Chromite	<i>Rhizopus oryzae</i>	
Galena	<i>Rhizopus oryzae</i>	
Plagioclase	<i>Rhizopus oryzae</i>	

The *Rhizopus oryzae* strain isolated from muscovite is conserved in the BCCM/IHEM collection as strain IHEM 22017, and the *Aspergillus flavus* strain isolated from sphalerite is conserved as strain IHEM 22016.

3.1.2. Three-Dimensional Colonization: Thigmotropism and Evidence of a Metalophagus Behavior?

Fungi densely colonized the surfaces of chromite, manganite, malachite, and galena but specifically showed a selective tangential hyphal growth pattern rather than a crossover longitudinal pattern. This tangential growth very frequently produced an envelope of fungal hyphae on all exposed mineral surfaces. As these surfaces represented planes intersecting in different orientations, most at $\sim 90^\circ$ and at a height well above the Petri dish base, the resulting colonization developed a definite 3D pattern (Figure 1a–d). Apparently, the 3D pattern of fungal growth and attachment to mineral surfaces occurred as a result of their ability to tangentially change growth direction at the intersection of mineral surfaces, perhaps signaling thigmotropic behavior in response to touch and physical contact with a solid surface. The outcome of this behavior is the total colonization of exposed mineral surfaces and increased surface area for fungal attachment, which, in turn, facilitates biochemical and biomechanical alterations of the former. For instance, Figure 1a (inset) shows the 3D colonization of a chromite chip having produced erosion and fragmentation at the sides of the exposed planes. Here, the 3D colonization and destruction of the chromite chip could suggest an incipient metalophagus process. Although nutrient invasive exploratory action of the fungal hyphae could be the reason for this behavior, we cannot exclude the possibility that the fungi responded defensively to some metal component in the substrate.

Figure 1e shows how the fungal hyphae envelope a grain of bauxite by changing their growth and bending along corners of the grain, which clearly appears strongly fragmented.

Figure 1f shows further the depth of the 3D colonization of the standing sides of a galena crystal. The change in growth direction is also clearly visible, along the corners and angles. In addition, densely colonizing all exposed sides, the fungal hyphae produced a thick layer of EPS material, within which are embedded finer hyphae. Interestingly, though, the smaller galena crystal to the left practically shows no colonization, perhaps reflecting selective colonization.

The ability of fungal hyphae to contour the mineral surface planes, changing growth direction at the angle of intersection to the mineral surfaces even when the angle is at 90° , is clearly displayed (Figure 2a,b), and so are chromite (Figure 2c) crystals. Here, the hyphae clearly display a specific contact-sensing behavior with respect to the mineral surface topography and probably also a spatial orientation. This behavior is further observed in Figure 2b, where after the hypha approaches the plane surface of galena; it creates an attachment anchor, then sharply reorients its growth direction further to the right or upwards at 90° and once more changes its growth direction tangentially along the new surface. It is interesting to note that the hypha approaches the mineral surface almost at $\sim 90^\circ$ before the attachment. The growing hyphal tip in Figure 2c further corroborates the above findings. At the abrupt intersection angle (also $\sim 90^\circ$), the tip sharply creates a bend over at the “cliff” and continues growth tangentially and in attachment downwards along

the new surface. Thigmotropism is further evident in Figure 3, where fully rounded and nondeflated fungal hyphae and tips growing on a Ca-plagioclase surface appear viable at least just before the SEM imaging. The hyphal tips are well attached to the natural mineral surface in the classical “nose-down” position of a “sniffing” hypha previously observed in fungi showing thigmotropic behavior (see [27] for similar behavior in *Aspergillus niger*).

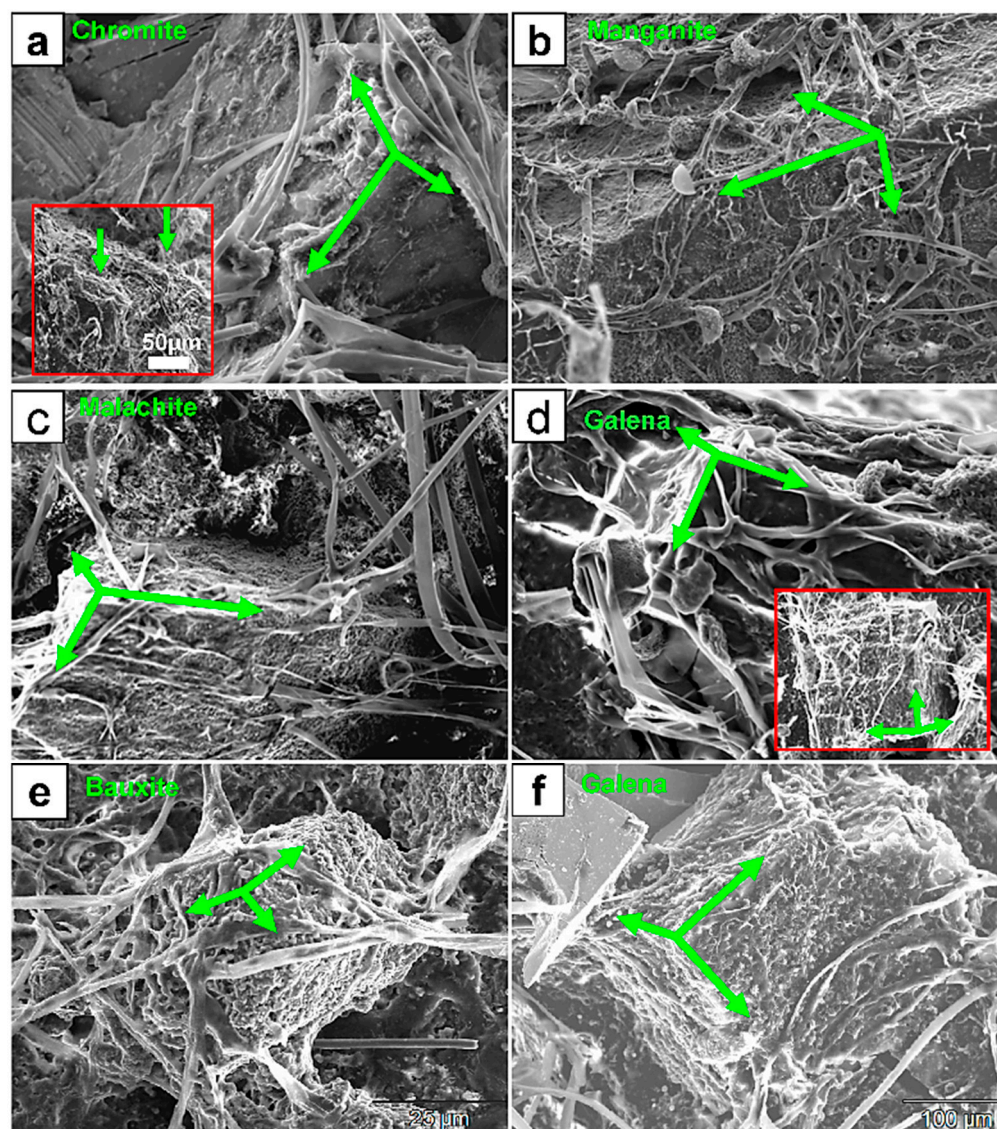


Figure 1. SEM micrographs showing examples of 3D colonization and thigmotropic behavior of fungi on mineral surfaces of chromite (a), manganite (b), malachite (c), bauxite (e), and galena (d,f). The extensive 3D fungal colonization occurred regardless of the substrate’s mineralogy, suggesting a metallophagous behavior. The intersecting green arrows in (a–f) point to the colonized metal surfaces in 3D. The colonization is not typically a longitudinal crossover but rather tangential, passing from one intersecting surface to another (green arrows) on the same crystal. This pattern even extends from one crystal to another, producing a 3D colonization pattern that envelops all exposed surfaces. The green arrows on all figures indicate the intersection in 3D of minerals surface exposed to fungal colonization. Note how the individual fungal hyphae grow from one surface to another while continuously adhering to those surfaces. The inset in (a) shows ridge-to-ridge 3D colonization and also the fungally digested ridges (green arrows).

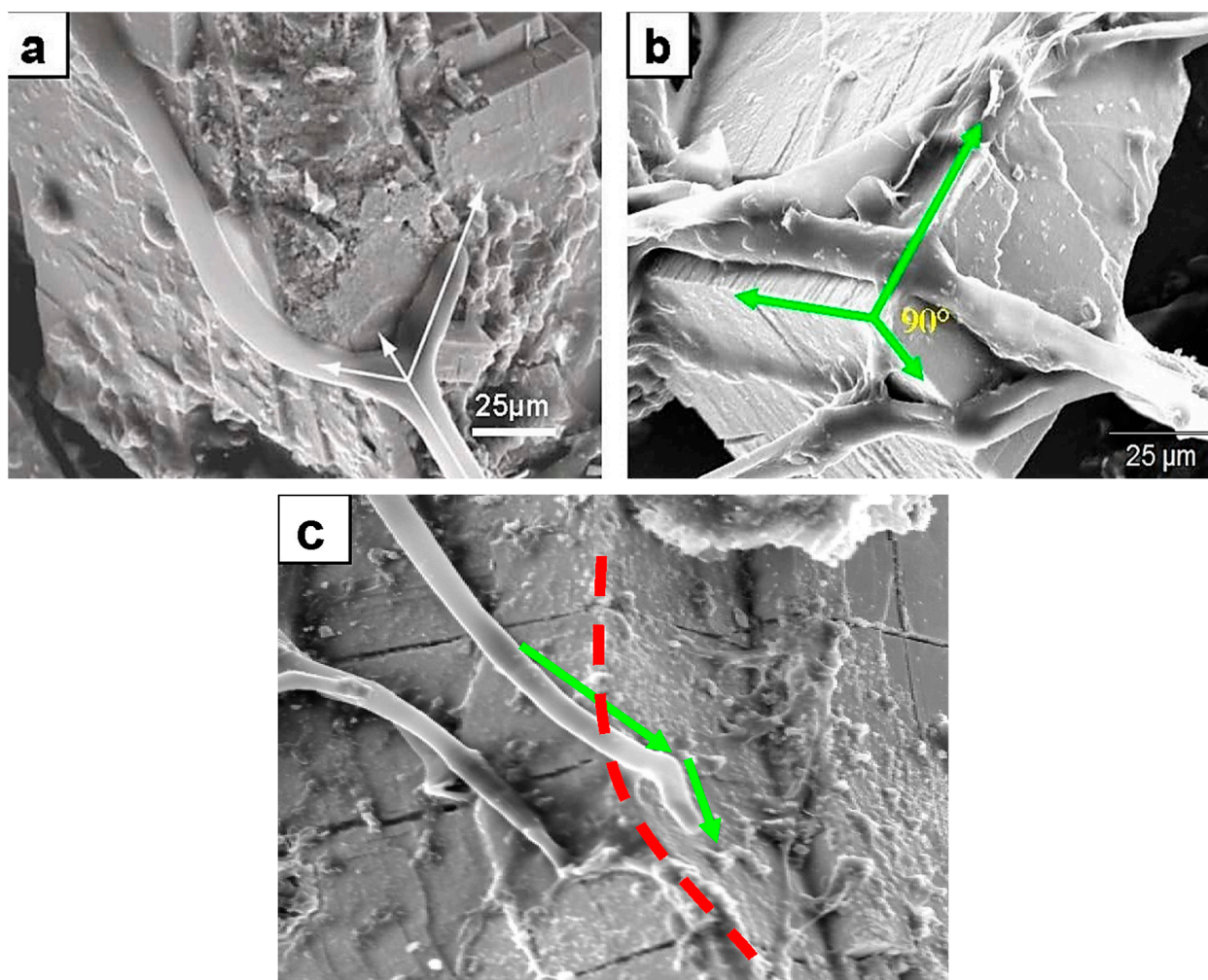


Figure 2. SEM images showing thigmotropic behavior of fungal hyphae during mineral colonization. (a) Branching of a hypha exactly at the intersecting planes of galena crystals. The dichotomy suggests a surface topographic sensing. The arrows point in the original growth direction before the meeting of the intersecting planes (middle arrow). The two new directional hyphal growths are following crystal planes. (b) Fungal hyphae anchoring on a galena mineral surface by EPS material, and the change of the hyphal growth direction at planes intersecting at 90° (green arrows). This is a quite significant thigmotropic behavior marking a topographic sensing not only of a horizontal plane surface but also of planes intersecting at very sharp angles. (c) Change in growth direction (green arrows) at crystal surfaces of an intersection on chromite (red dotted line). The three cases presented here are strongly suggestive of not only topographic sensing but, importantly, also 3D sensing of a growth environment.

The almost intact rhizoidal structure also shows hyphal rhizoids that practically follow the rugged mineral surface topography (lower mid-half of the image) and change growth direction accordingly. Indeed, there is evidence of at least two clear reorientations occurring at very short distances: a vertical one that follows the sharp angle ($\sim 90^\circ$) caused by two intersecting planes and a horizontal one that shows the hypha reorienting to avoid a topographic obstacle.

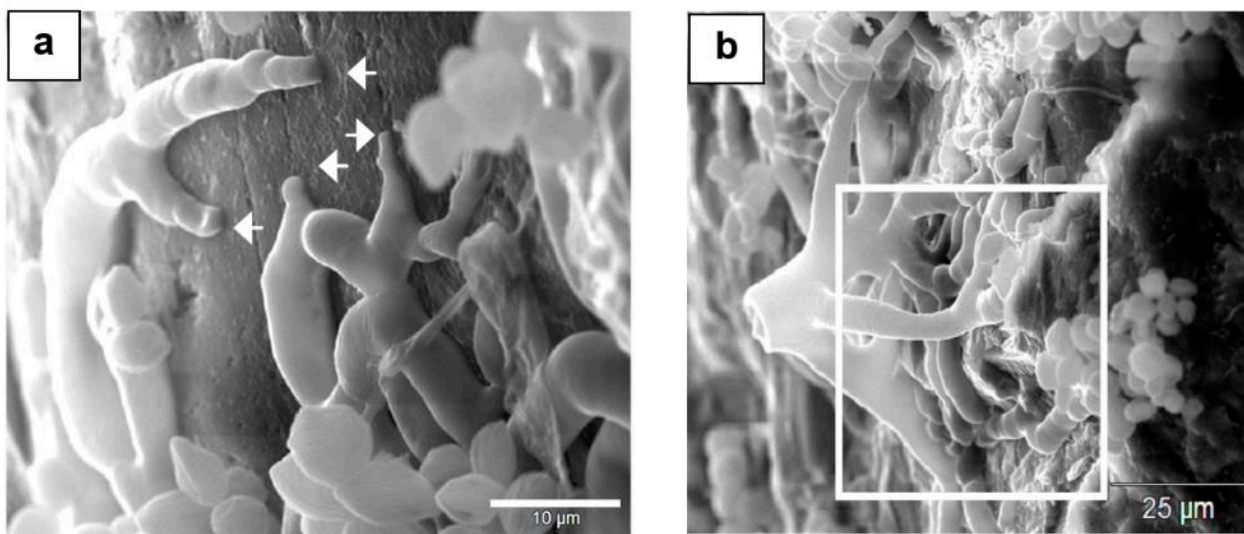


Figure 3. SEM images of fungal colonization of a mineral surface and their thigmotropic behavior: (a) Rounded nondeflated hyphal tips in a nose-down position growing on a plagioclase surface (short arrows) showing contact sensing. (b) Rhizoidal growth on the plagioclase substrate displaying contact sensing of the surface rugosity and topography (rectangle area).

In Figure 4, several fungal rhizoidal feet that ensure maximum adherence to the rugged surface further display thigmotropic behavior. The branching of the rhizoid in the center of Figure 4b occurs exactly at the elevated topography barrier, and this is of specific significance because it suggests the fungal “contact-sensing” ability of the mineral topography.

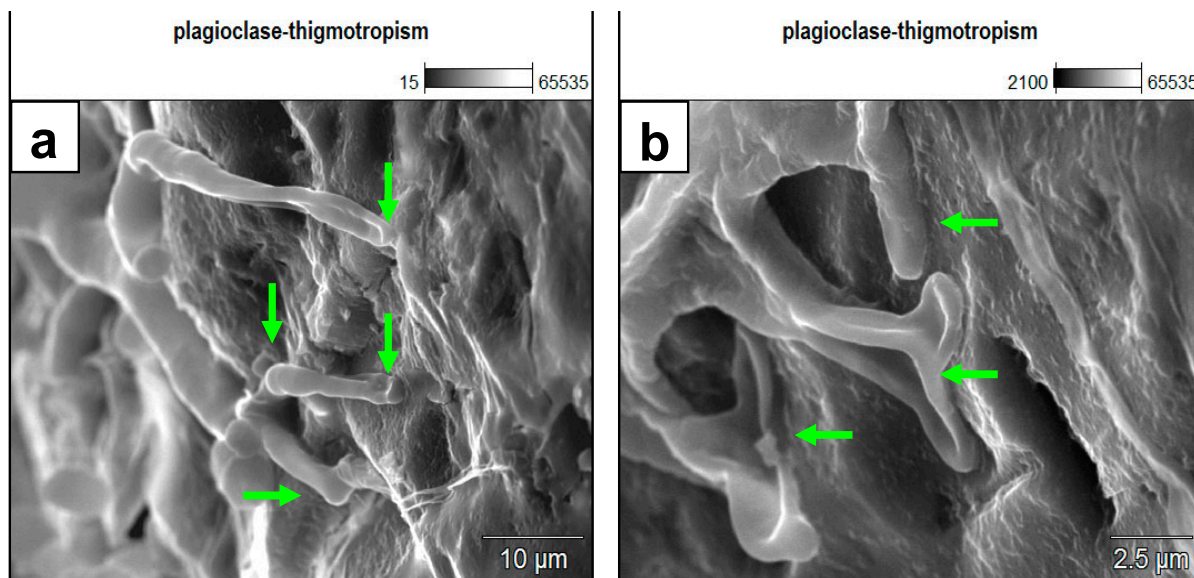


Figure 4. SEM images of rhizoids growth on plagioclase surfaces, displaying topographic and rugosity sensing behavior. Remarkably, the growth appears not to bypass the depressions on the mineral surface but rather fills in the depression. (a) The branching of a rhizoidal foot exactly at an elevated topographic barrier and filling the adjacent depressions further indicate thigmotropic behavior. (b) A detailed microscale (~2.5 μm) thigmotropic-sensing behavior of the fungal rhizoid responding to several topographic features of depressions and elevations on the plagioclase substrate surface. The arrows indicate points in contact with the substrate surface. The middle arrow is pointing to the characteristically significant dichotomy of the rhizoid foot at exactly an elevated feature separating two depressions.

3.1.3. Colonization of Smooth Surfaces: Muscovite and Biotite

Most minerals used in this experiment had rough surface textures, and through the process of cutting them into slabs and chips, they exposed a 3D topology. In contrast, muscovite and biotite were arranged in suspended horizontal and vertical positions well above the growth media to specifically test if there was a geometrical issue with regards to the fungal colonization patterns. Interestingly, the growing fungi nonetheless colonized these two micas. As there was no direct contact between the growth medium and the mineral surfaces (well above the Petri dish base), the hyphae of the growing fungi colonized the mineral surfaces through exploratory growth and attack. For instance, Figure 5a,b show “bushy” and dense mycelia of fungi colonizing the surfaces of two horizontally suspended sections of muscovite.

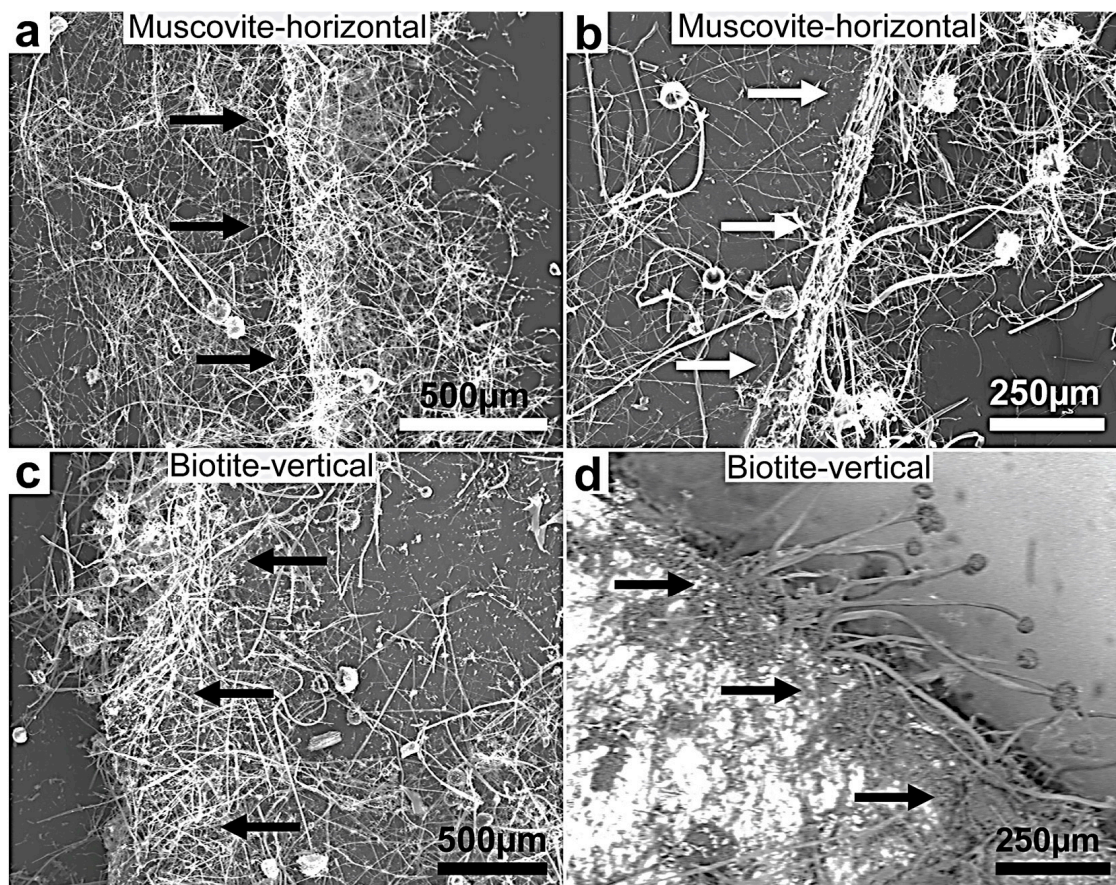


Figure 5. (a–d) SEM images of fungal growth and attack on muscovite and biotite showing more intensive growth on the two minerals’ multilamellar faces compared to the plane surfaces (the black and white arrows point in the direction of the preferential and intense fungal colonization growth at the biotite edges). This behavior shows a selective thigmotropic preference to attack and invade the points of weakness represented by the interlamellar bundle faces over the single plane surfaces irrespective of the position of the experimental lamellae, horizontally or vertically positioned. The growing hyphae showed a marked dense colonization of the substrata margin. (d) A backscattered image showing a clear contrast between the mineral surface (bright) and the organic biomass (dark grey). This selective growth indicates exceptional thigmotropic and metalophagus behavior.

Attachment, however, was selective, because it was consistently observed that the colonization and attack on the surfaces were more pronounced on the outer perimeter of the mineral sheets, specifically on the edges rather than the planar surfaces. In this regard, fungal hyphae appear to have invaded and colonized the thin lamellae in between their edges, and it is on these edges that mineral alteration is most pronounced. In some cases,

the colonization was very thin on the planar surfaces compared to the dense colonization on the edges. Under similar growth conditions, but with vertically aligned lamellae of both minerals, the colonization pattern repeated itself as in the horizontally aligned lamellae. The backscattered SEM image (Figure 5d) also shows the density of the dark-grayish growing fungi, many with clear sporangia, on the right side of the vertical Biotite plate compared to the nearly barren surface (bright area) of the plate.

3.2. Patterns of Mineral Substrate Alteration

3.2.1. Biochemical

General Metal Bioleaching. The 12-week experiment resulted in significant alteration of the mineral substrata. SEM, EDX, and XRD analyses showed metal enrichment on the fungal hyphae, secondary mineral mineralization (authigenesis), and clear biologically induced weathering patterns. The fungi interacted with all minerals, even galena, malachite, and bauxite, despite the toxicity of Pb, Cu, and Al, respectively, to fungal growth. One important aspect of these interactions is the strong affinity of fungal hyphae to mineral surfaces. In the first instance, EDX microanalyses of the fungal hyphae frequently revealed metals adsorbed onto the hyphae surfaces. The elements, including Fe, Pb, S, Cu, Al, Ca, and Mg (sourced from the mineral substrata and not from the medium, as described in Materials and Methods), were either deposited on the mineral surfaces, attached to fungal filaments, embedded in the fungal mycelium, or adsorbed onto the EPS. Metal enrichment subsequently led to the secondary biomineralization of several different crystal morphologies of Ca- and Mg-oxalates (weddelite, whewellite, and glushinskite); struvite; gibbsite ($\text{Al}(\text{OH})_3$); and possibly gypsum ($\text{CaSO}_4 \cdot 2\text{H}_2\text{O}$). Here, it is worthwhile to note that this mineral was formed during fungal interaction with the manganite ($\text{MnO}(\text{OH})$) substrate, which normally cannot be the source of Ca and S. This will be addressed individually in a subsequent section of the article. During the short period of the experiment, fungal interaction with the mineral surfaces also produced significant biomechanical and biochemical bioweathering features: strong pitting of the mineral surfaces, exfoliation, tunneling, dissolution, perforations, fragmentation, and cementation. Bauxite showed the most pronounced bioleaching patterns; Fe and Al were fungally leached and deposited as separate mineral species from the Al-Fe oxides mixture, and a unique pattern of pitting was produced on the mineral surface. The brownish-red, hard, and finely pisolitic bauxite samples were mainly composed of diaspore (AlOOH) and hematite.

Biotite and Muscovite. Strong metal bioleaching by the fungi was observed on biotite and muscovite. Al, Mg, Si, K, Ti, and Fe were leached from the biotite substrate and re-precipitated as a new separate mineral entity on either the biotite surface or within the fungal biomass. One prominent feature characterizing the leached elements was the apparent presence of a metal enrichment–depletion gradient between the biotite sheets and fungal biomass of the Al and Si elements from the biotite surface and enrichment towards the fungal biomass and newly formed authigenic mineral phases where the leached metals became concentrated. The EDX spectra (Figure 6b) were measured at short intervals on the lamellae surfaces where fungi had grown extensively.

They showed an increase in Si content across the transect point 1 to point 7; after which, Si dropped below detection in points 8 and 9. Aluminum and Mg behaved in a similar manner. Compared to these trends, Fe and Ti were removed from the substrate to a lesser degree, but still, their concentrations as reflected at the EDX peak height indicated a high-to-low gradient. The black mass in the middle of Figure 6a is a mixture of fungal biomass and newly formed minerals that shows a prismatic habit. Apparently, Al and Si were efficiently removed from the affected areas of biotite (zones 1 and 2 and 8 and 9), possibly through forming metal chelates with fungally produced organic acids.

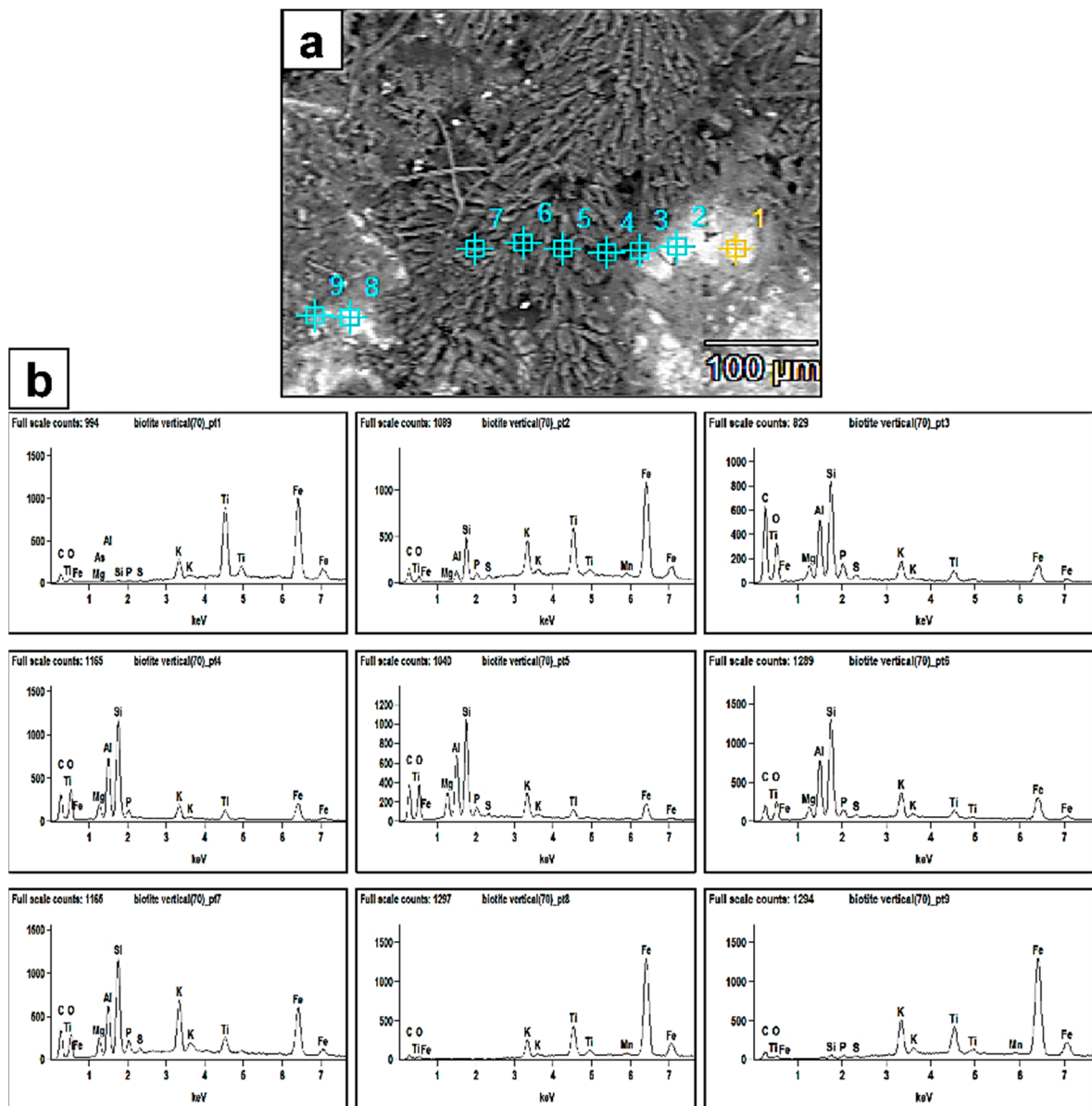


Figure 6. (a) SEM backscattered image revealing the extent of fungal biomass (dark grey) colonizing the biotite surface and also the biomineralized crystal aggregates (prismatic–tabular) associated with the biomass. The numbers represent the EDX analyses points. The bright areas are the biotite surface. (b) EDX spectra of points 1–9. The peaks clearly show more bioleaching of the Al and Si elements from the biotite surface and enrichment towards the fungal biomass and newly formed authigenic mineral phases.

In contrast to the bioleaching patterns exemplified by Figure 6, many elements are concentrated in the fungal biomass. For instance, Figure 7 shows an array of authigenic, tabular–prismatic crystals traversed by fungal hyphae and engulfed by spores. The EDX spectrum (Figure 7b) of these crystals (points 1 and 2) yielded strong peaks for Al, Mg, K, and Si, in addition to the presence of new elements C, O, P, S, and Ca. The superimposed EDX spectra of the biotite surface (point 3) and of the crystals indicate a biotite surface largely depleted in Mg, Al, and Si and, to a lower extent, in Fe, K, and Ti.

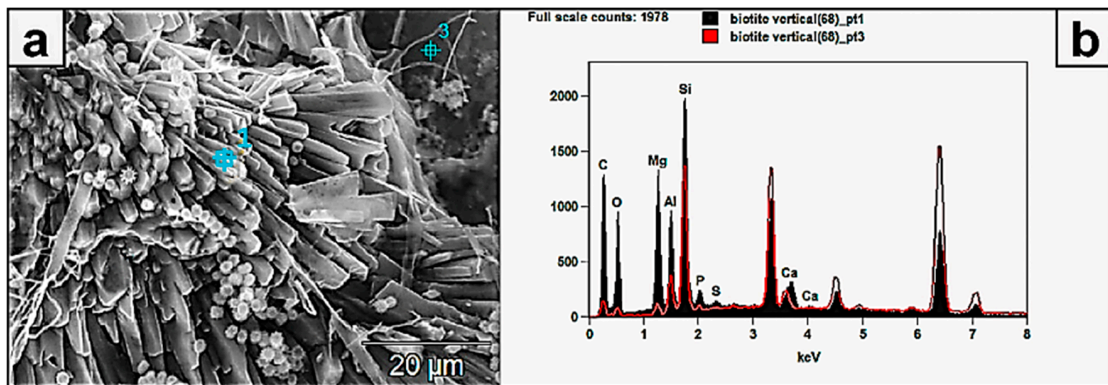


Figure 7. (a) SEM image showing the details of biomineralized prismatic–tabular crystals formed by fungal interaction with a biotite surface. Their composition reflects the major bioleached elements Si, Al, K, Fe, and Ti. (b) The spectra show relative mobility/leachability of Si and Al, because their peaks show higher intensity in the authigenic minerals than in the leached biotite substrate.

These trends corroborate the previously mentioned bioleaching gradient (Figure 6a,b). It is interesting to note the nearly total depletion of Mg from the biotite surface at the analysis point. These depletion/enrichment trends were repeatedly observed on several other locations of the biotite surfaces, enough to indicate a general trend of metal mobilization from the biotite towards the fungal mass, at least in the form of newly formed biominerals.

The role of fungi in biotite alteration and subsequent biomineralization is further evident in Figures 8 and 9.

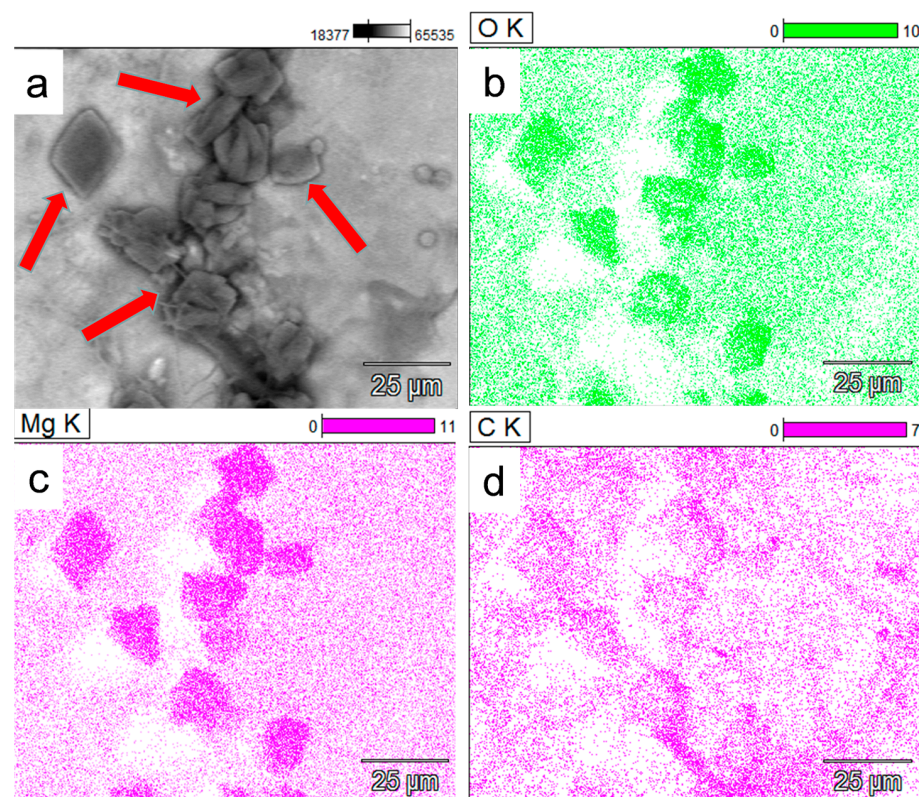


Figure 8. (a) SEM X-ray mapping image (backscattering mode) of authigenic minerals (black-greyish crystal forms) formed in response to fungal interaction with the biotite substrate (red arrows). (b–d) The new mineral crystals (the high color intensity shapes) depicted by the analysis to be mainly composed of O, Mg, and C, indicating the formation of Mg-oxalate mineral species MgC_2O_4 . The Mg is bioleached from the biotite mineral substrate.

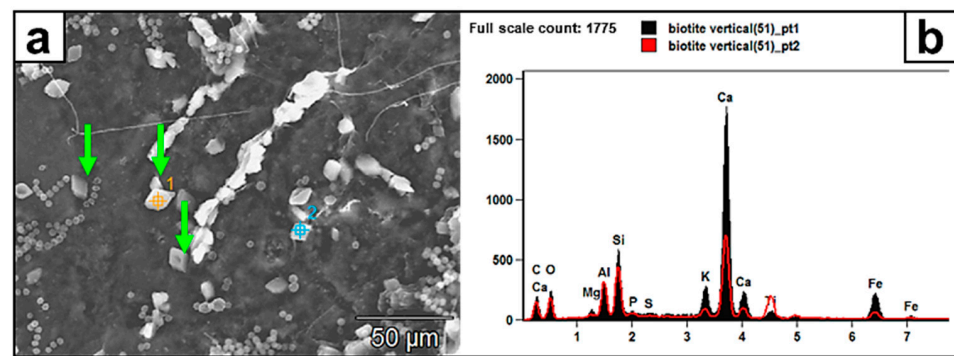


Figure 9. (a) SEM image of authigenic Ca-rich rhombohedral crystals (green arrows) deposited on the biotite surface and (b) the corresponding EDX pattern. These crystals, in absence of a mineralogical analysis, are likely poly-metal oxalates. Spot points 1 and 2 represent the EDX analyses of two crystals. The biotite surface appears scarred with pits and tunnels created by fungi.

The former shows crystals composed exclusively of Al, C, and O, likely gibbsite or an Al-oxalate mineral that are observed in direct contact with the biotite surface. In the latter, newly formed rhombohedral crystals, composed of Al, Mg, Si, Fe, and Ti, are seen in conjunction with pronounced bioweathering features on biotite, including surface tunneling and pitting.

Generally, muscovite displayed much lower bioleaching levels of Al and Si compared to biotite (Figures 10 and 11). In most cases, the levels of Al and Si seemed unchanged between the newly formed minerals and the muscovite substrate. In fact, even when the substrate was extensively altered, its elemental composition remained quasi-constant, as evidenced by the EDX analysis, apart from one single case where relatively strong peaks of Al and Si were recorded from newly formed crystals.

Bauxite. X-ray mapping and EDX analyses revealed Fe and Al concentrations directly related to a fungal leaching process. In Figure 12a (zone B, deep red area), there exists higher Fe concentrations within the area surrounded by highly dense fungal biomass (zones A and C and backscattered SEM inset figure) compared to the lower Fe outside this area, suggesting a strong leaching of Fe from the substrate and its accumulation in the area of fungal biomass activity. This relation is demonstrated clearly in Figure 12b, where the fungal biomass itself shows a higher concentration of Fe (inset X-ray mapping figure) compared to the surroundings. More direct evidence of Fe leaching is given in Figure 12c, where the leached Fe is not only concentrated, but it is also precipitated within the fungal mass as a separate layer on the original bauxite substrate and is composed of up to 87–93 wt% Fe (EDX analysis, Table 2). In lack of other analyses, the biologically precipitated iron possibly suggests an unoxidized native iron.

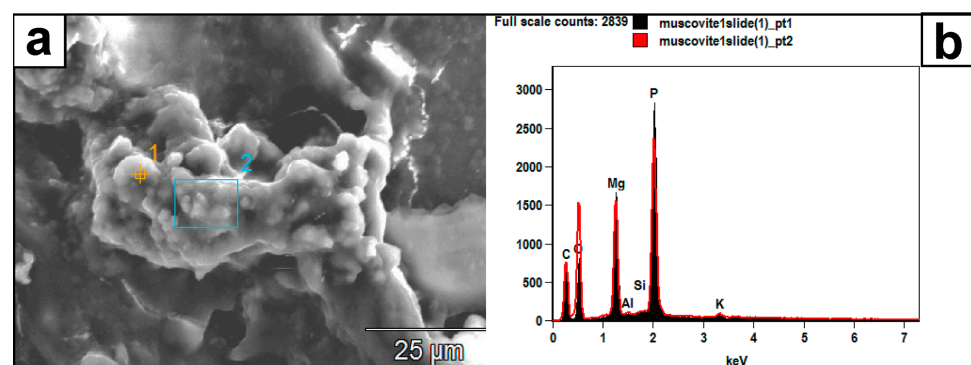


Figure 10. (a) SEM image of authigenic crystal aggregates formed on a muscovite surface and within a mass of EPS material. (b) Their EDX spectrum (pts. 1 and 2) reveals a composition of P, Mg, C, and O, which the muscovite substrate did not likely contribute. Instead, this composition might represent struvite: $(\text{NH}_4)\text{MgPO}_4 \cdot 6\text{H}_2\text{O}$.

Table 2. Quantitative EDX analysis of points 1 and 2 on precipitated iron.

Weight %	C	O	Al	Si	P	K	Ti	Fe
Bauxite_pt2	2.48		0.28	0.16		0.51	3.14	93.44
Bauxite_pt3	8.34	0.92		0.09	0.21	0.28	3.61	86.56

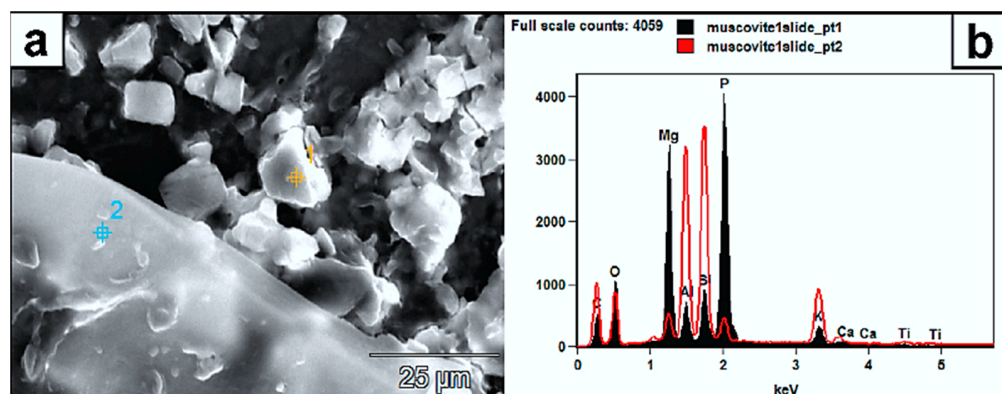


Figure 11. (a) SEM micrograph of authigenic mineral aggregates (white rhombs) formed on muscovite. (b) Their EDX spectra “pt1” reveals a composition of P, Mg, C, and O. In this single instance, Al, Si, and K are also mobilized from the substrate into the crystals. Point 2 is the muscovite EDX (red spectrum) and clearly shows the overall difference in elemental composition. Higher peaks are recorded here from the substrate for C and O due to the possible fungal material on the spot. The high intensity peak of P from the formed mineral can be sourced from the organic media; thus, compared to the muscovite EDX signature (point 2), the P is very low, and its existence is related to organic media as well. The high Mg signature in the newly formed mineral could reflect a higher mobility from the substrate.

Crystals directly associated with the fungal hyphae and EPS represent another form of bioleaching. They are composed of C-O-Ca-Al-Fe, with typical tetragonal bipyramidal forms characteristic of oxalates (Figure 12d). These authigenic minerals are not only enriched in Al and Fe (with EDX analyses yielding 4.87 and 11.6 wt% for Al and Fe, respectively) but also Ca (inset Figure 12f shows the very high EDX and XR mapping Ca signal of the hypha). Similarly, direct microanalysis of the hypha surface gave a high Al peak spectrum that was equal to 4.75 wt% of the total composition (Figure 12e). Moreover, the hypha was encrusted with neominerals in the form of oxalates, with the major elemental component being Ca (inset Figure 12f shows the very high EDX and XR mapping Ca signal of the hypha). The parallel area to the left of the hypha is also composed of high Ca in the form of fungally produced Ca-oxalates with similar composition to the crystals encrusting the hypha surface.

Manganite. Figure 13 shows Mn incorporation into the authigenic minerals coating the fungal hyphae and also within the EPS formed on the original manganite surface, which also contains biominerals (Figure 13a—arrows: EDX zones 2 and 3). Figure 13b shows a SEM backscattered image where biominerals encrust the hyphae surface and litter the underlying substratum as well. These crystals and the EPS, collectively or singularly, are the source of the Mn signal detected by the EDX analysis on the hyphae surface (Figure 13a, zone 5 and Figure 13b, zone 1), which yielded 4.30 wt% and 2.0 wt% Mn, respectively, while it reached 27 wt% Mn on EPS zones 2 and 3 (Figure 13a), suggesting more active leaching of the manganite surface in this region. The Ca-containing prismatic bipyramidal crystals in Figure 13b are typical Ca-oxalates that either encrusted the fungal hyphae or were deposited as free crystals on the mineral substrate, but the small Mn signal in their EDX spectrum suggests a possible complex metal oxalate of Ca and $\text{Mn-C}_2\text{O}_4 \cdot 2\text{H}_2\text{O}$.

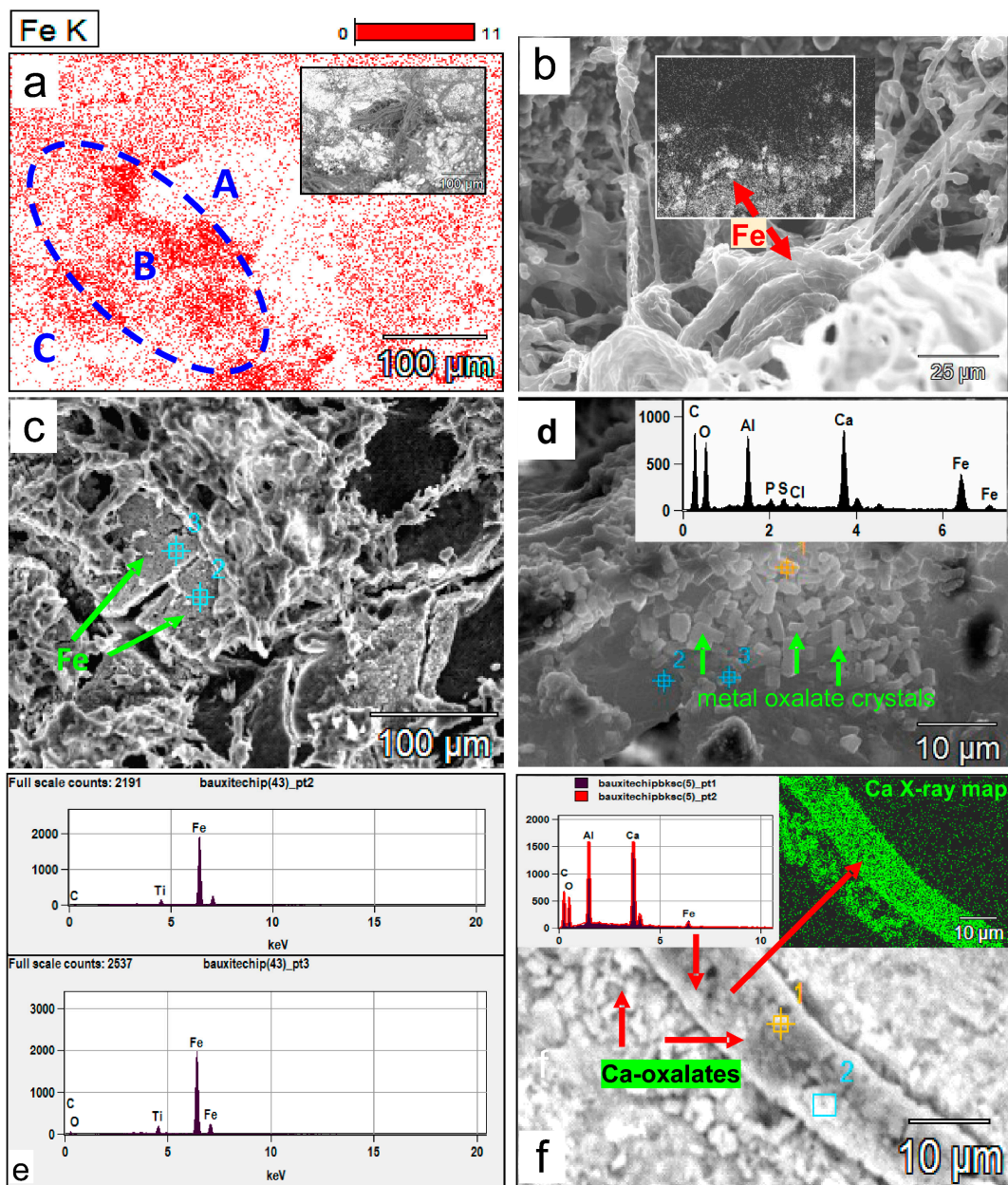


Figure 12. (a) SEM X-Ray mapping of Fe on a bauxite surface densely colonized by fungi (zones A and C and inset figure for the corresponding areas), showing that high Fe concentrations in zone B are related to the presence of a dense fungal biomass in contrast to the lower Fe concentration associated with the rest of the map. The white areas indicate fungal biomass, as is the SEM backscattered inset figure. (b) A high concentration of Fe (inset backscattering map, the red arrow indicating the same iron enriched area) is contained within the fungal mass itself compared to the surroundings. (c) Bioleached Fe (red arrows) forms a separate layer of spongy and porous Fe mineral within the fungal biomass. The EDX spectra of points 1 and 2 (e) indicate Fe makes up to 87–93 wt% of this layer. (d) Prismatic tetragonal bipyramidal crystal aggregates (arrows) formed in or within fungal mucilaginous material that contain Al and Fe; metals presumably bioleached from the substrate bauxite and now incorporated into a Ca-Al-Fe-oxalate complex shown in the inset EDX spectrum of spot point 1. (e) EDX spectra of spot points 2 and 3 on the iron-rich layer bioleached from bauxite in (c). (f) The role of fungal hyphae in bioleaching. Biom mineralized crystals encrusting a hypha yielded an EDX spectrum with strong Al and Ca peaks and low Fe. The high Ca crystals on hyphae and deposited parallel to the hyphae are likely Ca- and Al-oxalates (red arrows point to the EDX spectra of spot points 1 and 2 on the X-ray map of Ca in crystals encrusting the fungal hypha).

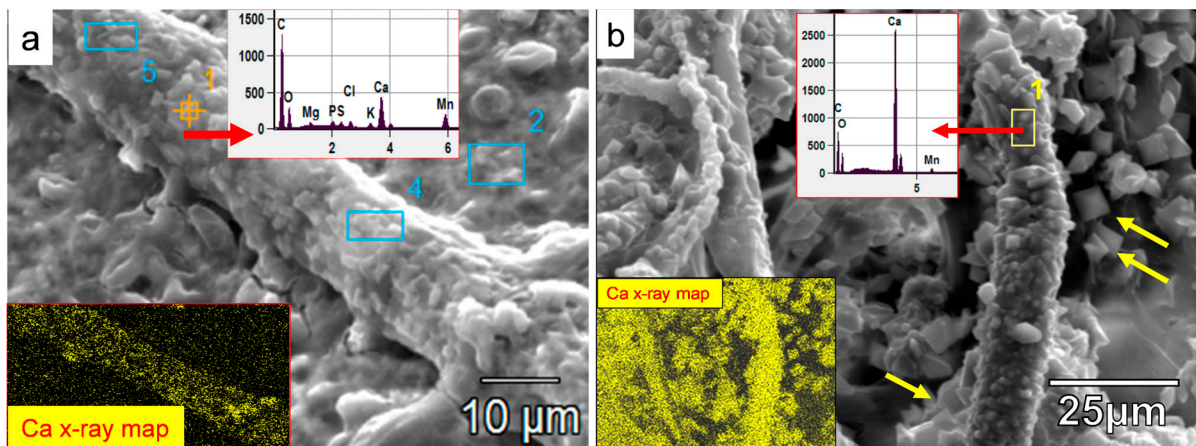


Figure 13. SEM images of authigenic crystals densely encrusting the fungal hyphae in (a,b) and littering the surface of the manganite substrate. (a) The substrate, as well as the hypha, are intermixed with EPS material. The hypha is densely encrusted with mineral crystals formed during the interaction with the substrate. The typical EDX signature (inset, above and arrow of analyzed spot 1) shows a mainly Ca-dominated composition with minor contributions from other elements, specifically Mn. The lower inset shows the Ca makeup of those encrusting minerals. (b) EPS material is not clearly visible. The fungal hyphae are more densely encrusted, with well-formed Ca-oxalates with a very minor contribution of fungally leached Mn (EDX spectrum inset and area analyzed in rectangle 1) from the substrate and subsequently incorporated in the Ca-rich crystals, which represent a mixed metal oxalate ($\text{CaMnC}_2\text{O}_4 \cdot 2\text{H}_2\text{O}$). The X-ray map of Ca shows the extent of the dense encrustation and of the fungal hyphae by the Ca-oxalates. The yellow arrows are pointing to typical prismatic bipyramidal tetragonal crystal shapes of Ca-oxalates. (Blue rectangles in (a) are other EDX analyzed areas of similar spectrum as for spot point 1).

Malachite. Fine (2–3 μm) authigenic crystals encrust the fungal hyphae that colonized the malachite surface. EDX analysis of these crystals yielded a Cu content of between 24 and 25 wt% (Figure 14a,b, zones 1 and point 1). These values are quite high and represent an efficient incorporation of Cu bioleached from the malachite substrate into the newly formed minerals encrusting the fungal hyphae. By contrast, authigenic minerals were not observed on the malachite surface itself, seemingly implying that mineral nucleation occurred preferentially on organic ligands.

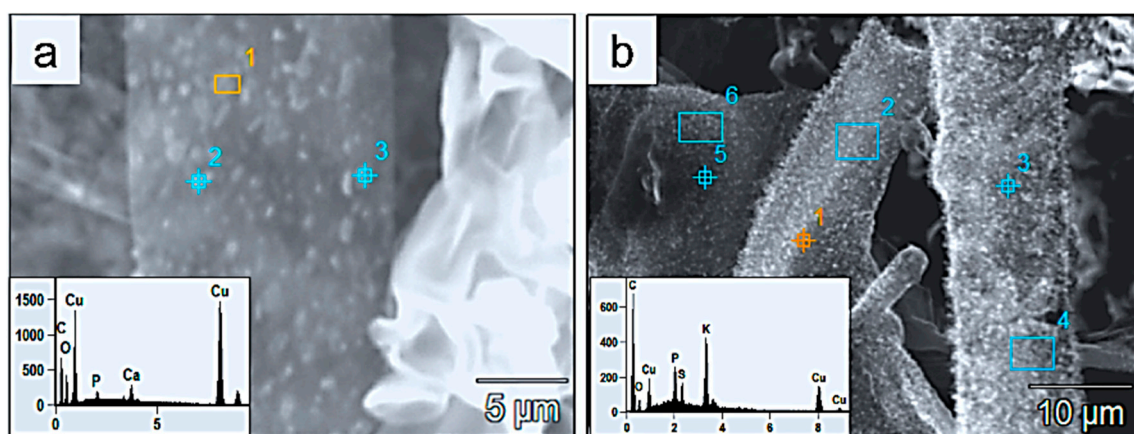


Figure 14. SEM micrographs and EDX analyses. (a) Area 1 and (b) spot 1 of fine-grained crystals (2–3 μm) formed on fungal hyphae and displaying high Cu% that was leached from the malachite substrate and adsorbed onto the hyphal walls and encrusting crystals. (Blue spot points and rectangles in (a,b) are additional EDX analyses of similar spectra).

Chromite. Chromium (and Fe) was leached from the chromite substrate and reincorporated into newly formed mineral crystals, probably as an oxalate complex. Figure 15 shows clusters of authigenic crystals embedded in fungal EPS. The EDX spectrum of the crystals shows strong Cr (up to 16 wt%), Fe, and Ca peaks.

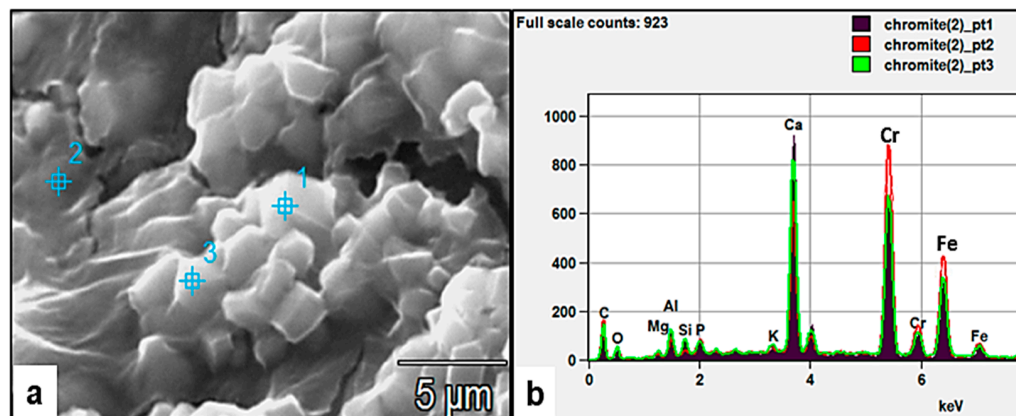


Figure 15. (a) SEM images of clusters of fungally produced rhombic crystals embedded in EPS and comprising Cr, Fe, and Ca (as evident in the EDX spectra (b) of spot points analyses 1–3 in (a)). The association of the crystals with the fungal EPS (point 1 and 3) material suggests the preferential sorption of Cr to the biomass.

Galena. SEM-EDX analyses (Figure 16) show that both Pb and S were leached from galena and incorporated into the fungal biomass. An EDX spectrum of the separate hyphal biomass (dark grey) above the galena surface (bright white-grey), but not directly attached to the mineral surface, shows a composition of C, O, P, K, Ca, Pb, and S, which suggests, in this instance, that both Pb and S were solubilized, mobilized, and then incorporated from the galena into the fungal hyphae. The galena EDX signal shows no Ca, K, P, Mg, C, or O; instead, its signal is representative of the pure sulfide phase. On a magnified scale, several EDX analyses of the fungal hyphae attached to a galena crystal (in Figure 16b) confirm Pb and S mobilization from the galena substrate and their incorporation within the hyphal wall. The size of the hypha ensures that the source of the analyzed signal is from the hypha surface and not the underlying galena surface. In many cases, the fungal hyphae produced blackened tracks on the exposed smooth galena surface parallel to their growth (Figure 16c, arrows). The hyphae are well attached to the surfaces and apparently also show some dipping into the mineral surface. These black tracks, which are only associated with attached hyphae, suggest a zonal reaction between the fungal exudates (organic acids) and the mineral surface, causing its oxidation and blackening and also its bioleaching; in this case, S and Pb.

The X-ray mapping of some colonized galena crystal surface also displays variable concentration intensities for Pb and S on the galena surface (Figure 17a–c); the white areas (Figure 17b,c, arrows) indicate depleted and oxidized zones where lower concentrations of Pb and S were detected, while the high-intensity colored zones represent the original nondepleted surface. In the backscattered SEM image (Figure 17a), the blackish-greyish areas on galena crystal surface represent the areas affected by fungal colonization, and they extend beyond the direct attachment zones of the fungal material (see also Figure 17c), thus, in this case, creating a halo around these reaction zones. This reaction halo is clearly presented in Figure 17d,f, where it is still possible in normal SEM image mode (Figure 17d) to differentiate the fungal biomass from the reaction area. The excretion of organic products by the fungi has likely affected areas adjacent to the fungal biomass; no liquid reactants were added to the mineral surface during the experiment, but rather, the colonization of galena surfaces occurred well above the growth medium, and thus, the reaction areas that extended beyond direct fungal contact with the galena surface must have developed in

response to the excretion of fungal exudates. The EDX spectrum in Figure 17e shows Pb and S depletion in the colonized area compared to the original surface.

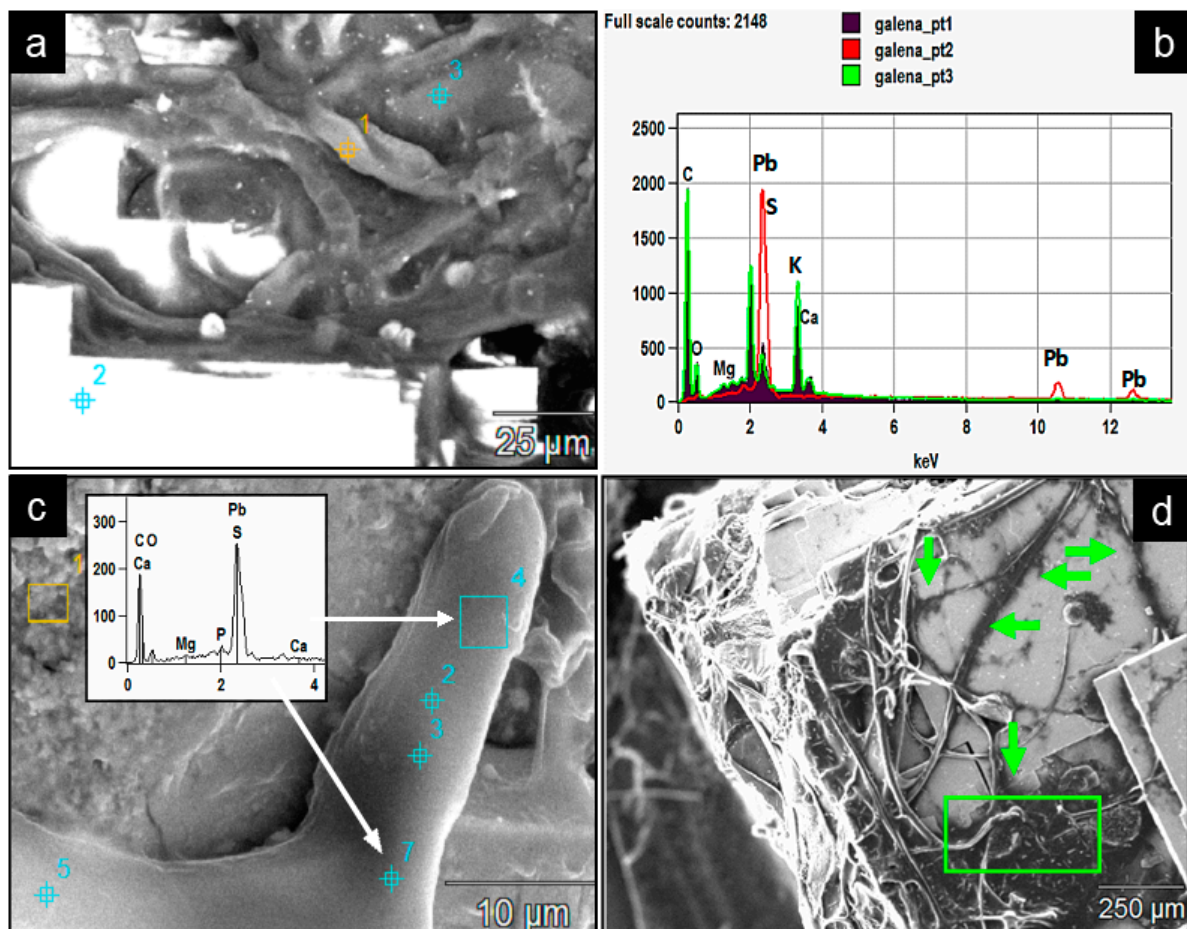


Figure 16. (a) SEM backscattered image of a fungal biomass (dark grey) colonizing galena crystal surface (bright white). (b) The EDX spectra of the three analyzed spot points in (a) within the fungal mass (1 and 3) and galena crystal surface (2) show Pb, S enrichment and the original galena elemental composition respectively. (c) A detailed EDX analysis of the hypha from two representative analyzed area 4 (blue rectangle) and spot point 7. The spectrum strongly suggests the leaching of Pb and S from colonized galena surface into the hypha. (d) Fungal hyphae are embedded in black areas (green arrows and the rectangle), suggesting a possible reaction–depletion process around the fungal hyphae colonizing the galena surface.

Plagioclase. Prismatic and tabular crystals formed on the plagioclase surface following fungal interaction (Figure 18a). The EDX analysis of these crystals yielded a composition of major elements (Al, Si, Ca, and K) similar to that of the Ca-plagioclase substrate (Figure 18b). Indeed, the plagioclase was the only source for these elements.

The overlain spectrum shows the difference in peak intensity of these elements compared at two locations: the prismatic crystals (point of analysis 1) and plagioclase surface (point of analysis 4). The other analysis points gave similar results. The calculated weight percentages (Table 3) suggest the leached wt% of each element is relative to its wt% in the plagioclase substrate. This applies to the wt% ratios (crystal/substrate) of Ca: 2.5/32.4, Si: 1.45/29.79, and Al: 0.85/7.02, but K signals a high leached ratio of 1.32/2.37. The latter suggests a possible higher leachability of K or the presence of a second source besides the plagioclase substrate, which is the organic growth medium. This latter source might also explain the presence of P and S that do not appear in the composition of the plagioclase substrate yet form part of the authigenically formed crystals.

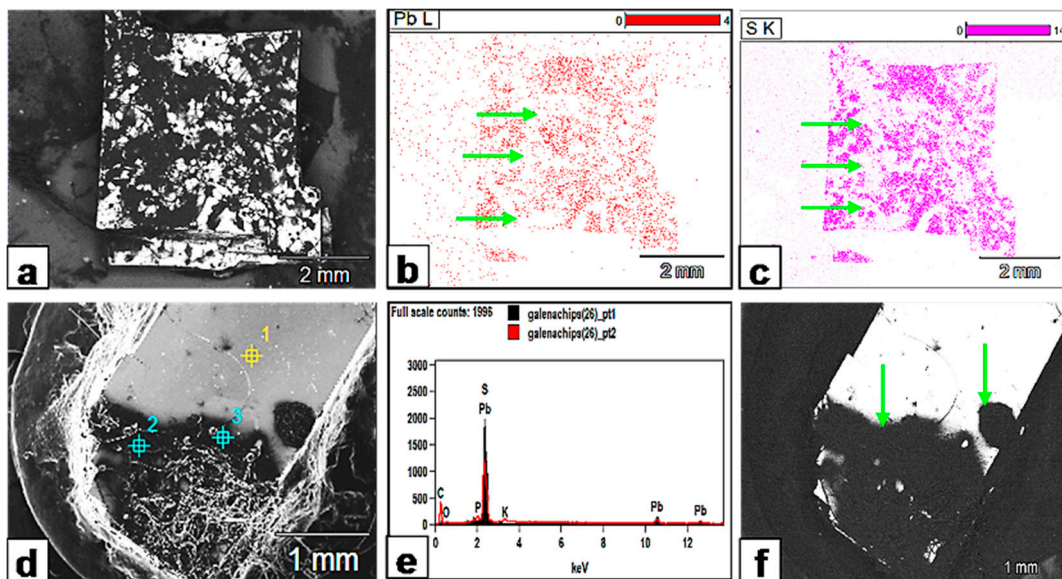


Figure 17. Metal bioleaching from galena. (a) SEM backscattered image showing the extent of the fungally affected areas (black) on galena. (b,c) XR mapping of the galena crystal surface shows that the black areas in (a) (fungally attacked) are quite depleted in both Pb and S and appear as white zones (green arrows) on the XR maps (compare the same areas with the black counterparts in (a)). (d) SEM image showing that the fungally attacked areas (black) extend beyond the fungal hypha or biomass and create a halo around it. (e) The EDX analysis of spot points 1 (yellow) and 2 (blue) on the crystal surface (d) confirms Pb and S depletion. (f) SEM backscattered image reveals how the whole area (green arrows) is affected by fungal exudates and appears as one reaction zone.

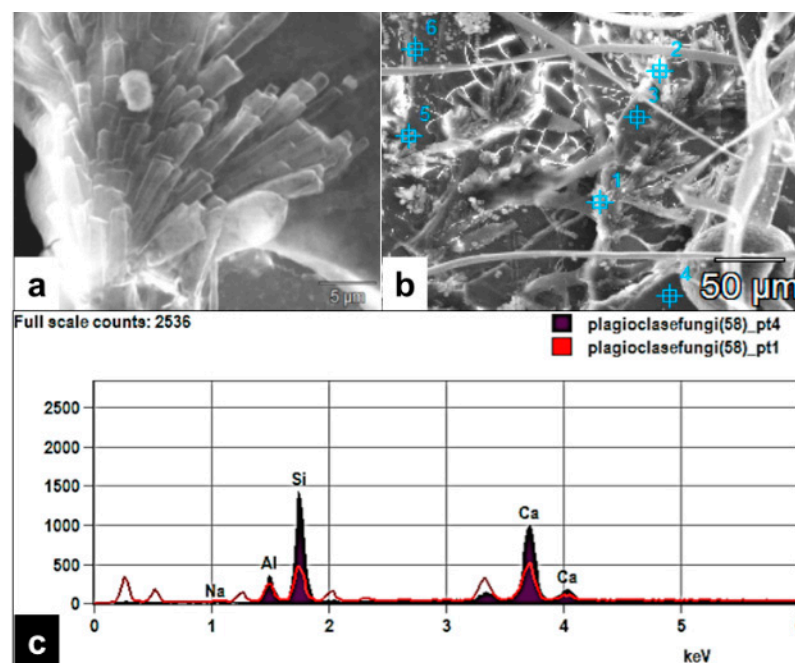


Figure 18. Bioleaching of plagioclase. (a) Prismatic–tabular crystals are formed on the plagioclase surface within the colonizing fungal biomass (b). (b) The fungal mass colonizing the plagioclase with different EDX spot analyses (blues points 1–6). (c) EDX spot analysis spectra of points 1 and 4 in (b) depicting the bioleaching of Al, Si and Ca from the plagioclase substrate into the fungal mass. Their chemical composition reflects the main components of plagioclase: Al, Si, Ca, and K.

Table 3. EDX analysis of the prismatic crystal aggregates (point 1) and plagioclase substrate (point 4) in the figure (image).

Weight %	C	O	Mg	Al	Si	P	S	K	Ca
EDX of Prismatic crystals aggregate: point 1	24.08	68.81	0.5	0.85	1.45	0.39	0.1	1.32	2.5
EDX Plagioclase substrate point 4	18.17	6.91		7.02	29.79			2.37	32.4

3.2.2. Combined Biochemical/Biomechanical

Exfoliation and Fragmentation. A number of the mineral samples showed evidence of exfoliation, the process whereby layers from the uppermost mineral or rock surface are successively removed from the underlying substratum. In galena, single or sometimes multiple thin exfoliated layers (0.5–1.0 μm) were visible (Figure 19a,b), parting parallel to the cleavage surfaces, while the exfoliation of muscovite (Figure 20c) and biotite (Figure 20d) occurred in the form of fine fragmented chips displaying a whitish color.

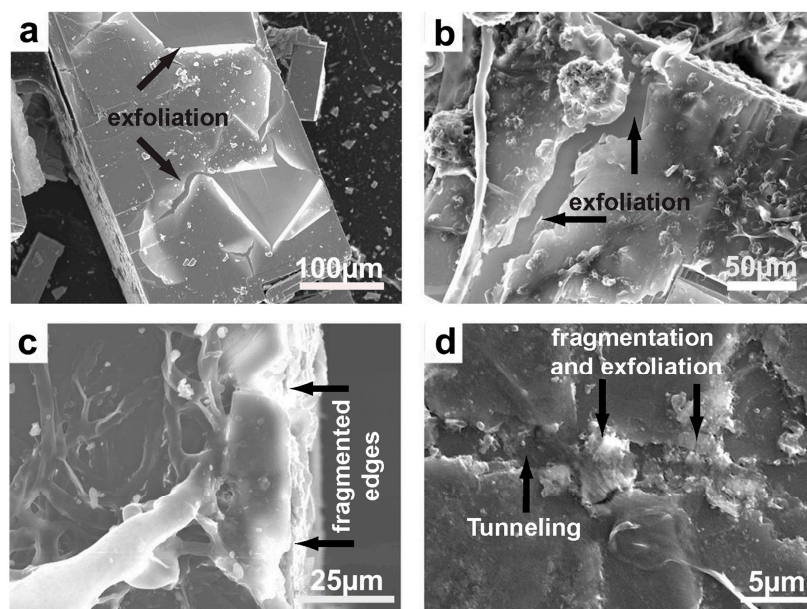


Figure 19. SEM images of exfoliation and fragmentation of the mineral substrata. (a,b) Galena crystals displaying pronounced exfoliation and parting along the cleavage planes following fungal colonization. (c) Muscovite lamellae displaying severe fragmentation on the edges. (d) Biotite surface showing tunneling and fragmentation.

It is likely that the mechanism for exfoliation occurred through mineral solubilization by organic acid exudates combined with grain dislodgement by biomechanical forces of the probing hyphae. In other examples (Figure 20a), solubilization appeared to result in severe fragmentation, such as in the cases of manganite (Figure 20a), malachite (Figure 20b), and chromite (Figure 20c,d). The manganite chip is entirely transformed into a friable powdery mass that still shows colonizing fungal hyphae intercalating and penetrating the fragmented mineral. Also present are abundant authigenic mineral grains (white and fine crystals). Similarly, malachite displays strong fragmentation and fungal colonization, which has produced deep grooves on the mineral surface, leaving a columned appearance that perhaps reflects its original prismatic crystal habit only accentuated by fungal biochemical activity.

Figure 20c,d show a strongly fragmented chromite crystal with fine residues covering the crystal surface. One single hypha is shown penetrating through the crystal (Figure 20d), although the original sharp crystal lineaments are obscured and the crystal surface, as well as the altered corner, is richly covered in EPS and fungal hyphae. Here, again, the whitish fine material represents a secondary mineral formation by fungal activity. The

plagioclase has been severely degraded by fungal action, and the surface appears corroded and fragmented. Its surface is covered in prismatic crystals (Figure 20e, inset). Interestingly, the fungal hyphae appear to be encrusted with acicular, thorn-like crystals.

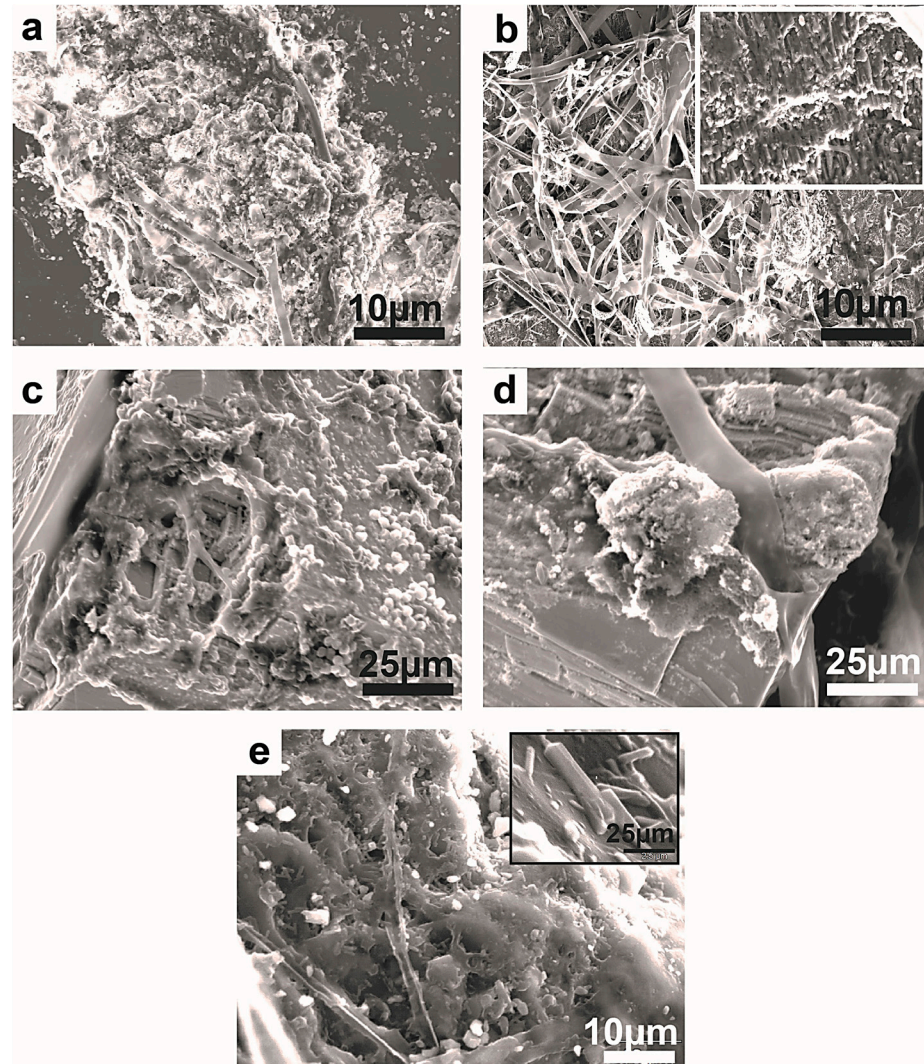


Figure 20. SEM images showing fragmentation of the mineral substrata. (a) Severely fragmented manganite substrate still showing the invading fungal hyphae. (b) The densely colonized malachite is grooved and scarred by fungal hyphae and, on the surface, the secondary precipitation of authigenic mineral phases (inset figure). (c) The densely colonized chromite substrate displays strong degradation at its corner. (d) Similar degradation and fragmentation on chromite shows a powdery material as a result of fungal attack. The single vertical hyphae appear to have perforated the chromite crystal. (c,d) The crystal lineaments are obscured by the fungal interaction with the substrate. (e) Plagioclase showing pitting and fragmentation following the fungal colonization. Its surface is littered with prismatic crystal that formed as secondary minerals with elements leached from the substrate.

Tunneling. Tunneling is defined here as horizontal or vertical “burrows” made by fungi into the mineral substrate [28,29]. On the biotite and muscovite surfaces (Figure 21), the fungi produced a specific pattern of sawtooth-serrated features that run along the mineral surface with variable sizes (2.5–10 μm wide, ~0.5 μm deep, with a visible length in excess of 80 μm). In some instances, it is possible to observe a mineral alteration product that has accumulated at equal length segments (~100 μm) inside the burrows that resemble septation (e.g., Figure 21b). These mineral accumulations occur at the narrowing rounded neck end, which is followed by a widening that starts the next segment. This could indicate

the direction of fungal tip growth (hence the tunneling direction) and, possibly, pulsated growth patterns.

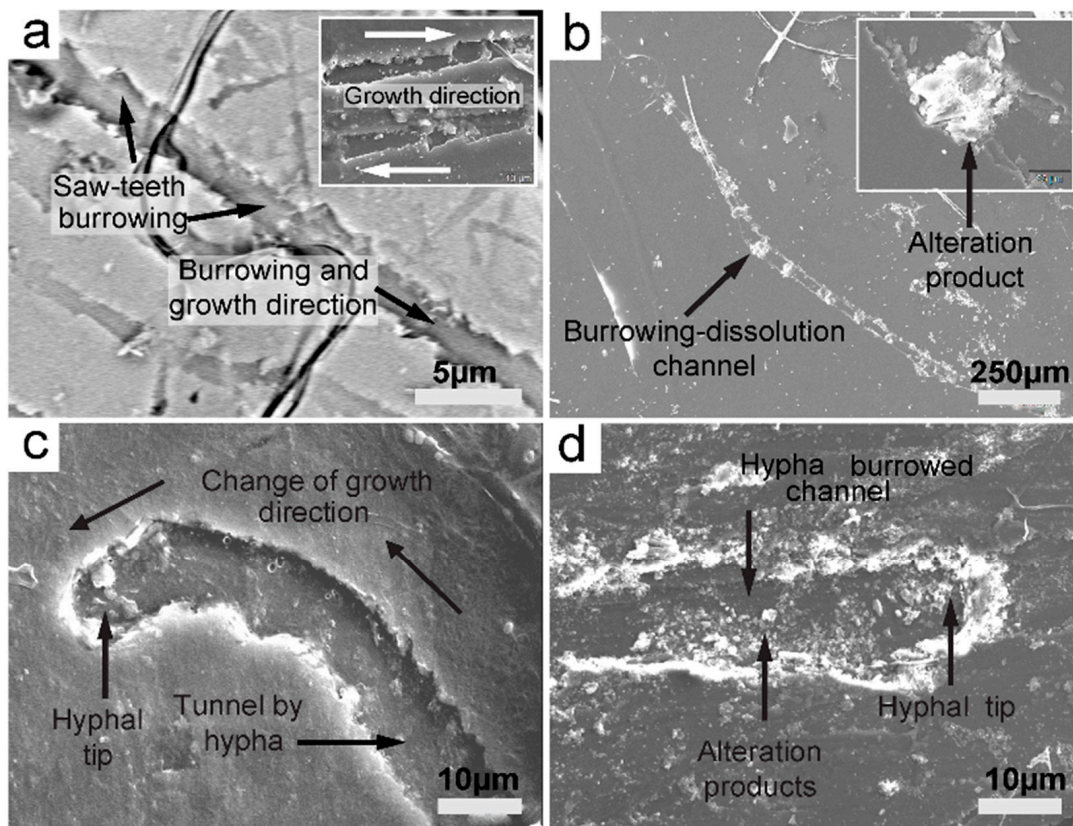


Figure 21. SEM images of fungal hyphae displaying saw teeth tunneling into various mineral substrata. (a) Fungal sawtooth burrows into biotite, creating a network of channels. (b) A burrowed channel showing alteration products at equal length segments, probably septation locations on the fungal hyphae on biotite. (c) A clear case of fungal tunneling of a biotite surface displaying a hyphal tip and, importantly, a change in growth direction: a thigmotropic response. (d) Burrowed channel with rich alteration products and a hyphal tip on muscovite. (a) Backscattered mode.

This is further demonstrated in Figure 21c, where the clear curving of the hyphal tip indicates both growth and the tunneling direction of the hypha into biotite. Some alteration mineral products have accumulated at the hyphal tip. A similar hyphal tip is observed in muscovite (Figure 21d), with alteration and tunneling products littering the burrow. One important aspect of these tunneling features is that they are restricted to the experimental vertically oriented plates of both biotite and muscovite. Fungi interacted differently with horizontally placed plates.

Figure 22a shows a fungal hypha (a germ tube) growing from a *Rhizopus oryzae* spore at one end and penetrating biotite at the other end to about 10µm. Similar oriented growth is observed in Figure 23b. Although the images show a certain angle of penetration, Figure 23b clearly reveals a vertical entrance of fungal hypha, probably due to oriented apical growth. This would also imply certain recognition of the mineral substrate. In muscovite, the branching hypha (Figure 22c) penetrates the substrate at an angle and partially disappears below substrate surface, leaving a trace shadow of the tunnel and the clear end of the hyphal tip. The gradual perforation and tunneling is also evidenced in Figure 22d, where a hypha is observed inclined to the surface and gradually sinking below the surface until the fungal tip eventually disappears to continue growth below the substrate surface. A similar case is demonstrated in Figure 22e, where the hyphal tip penetrates the muscovite substrate. Tunneling could also show pitting or a “burrow

entrance” (Figure 22d), which possibly indicates the penetration location of the hypha. The differentiated fungal growth pattern (surface burrowing vs. real tunneling and vertical perforations) in vertically or horizontally oriented mineral surfaces of muscovite and biotite suggests a gravitropic response to mineral spatial arrangement. Gravitropism has been demonstrated in certain fungi (e.g., Basidiomycetes and zygomycetes) [30–32].

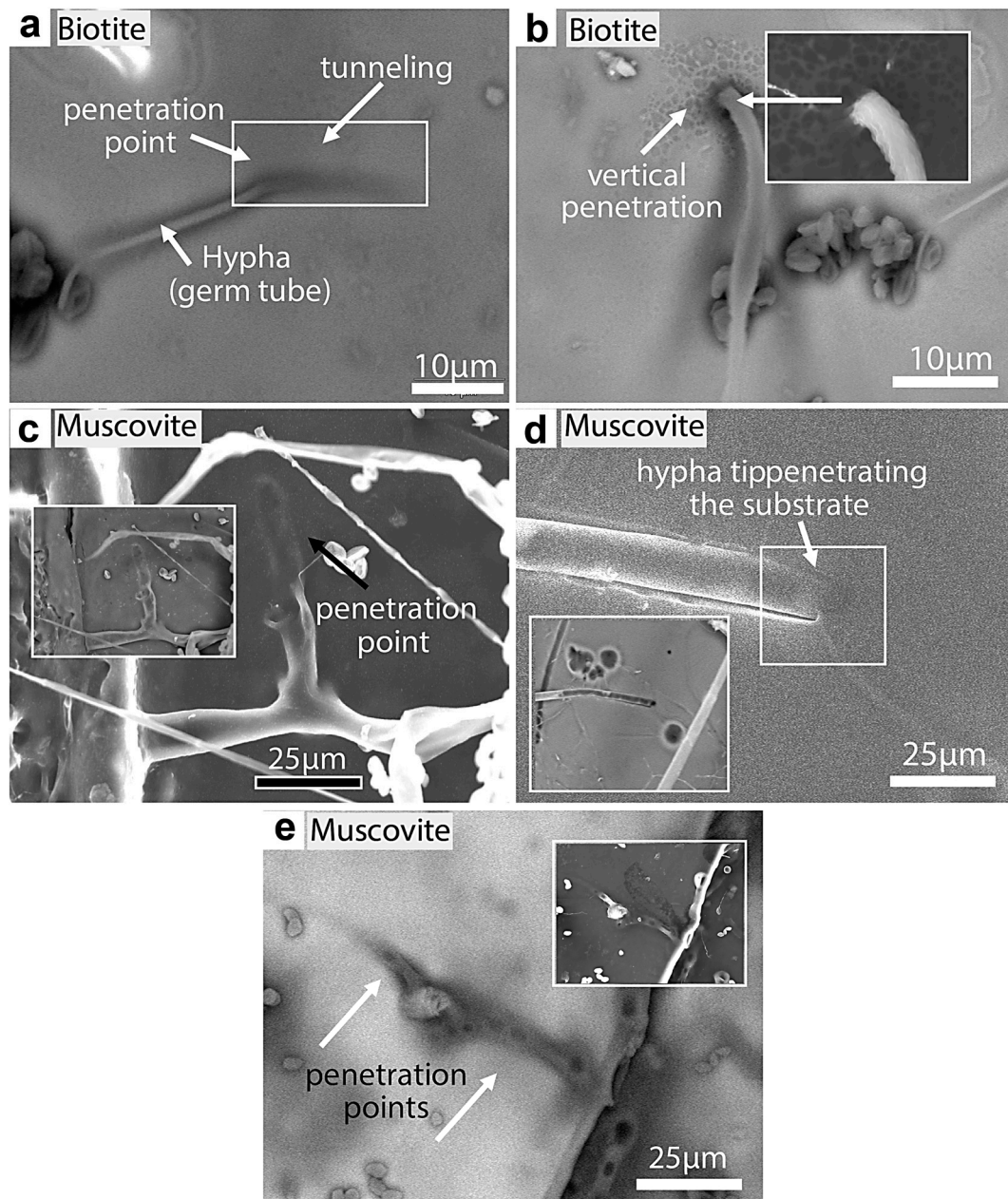


Figure 22. SEM images of fungal tunneling into biotite and muscovite. (a) A germ tube (*Rhizopus oryzae*) tunneling into a biotite substrate at an inclined angle. (b) Hypha vertically penetrating biotite. (c) Hypha branching and tunneling into muscovite (shadow traces of penetration). (d) Hypha showing gradual tunneling and the disappearance of the hyphal tip below the muscovite surface (BKSC image shows the black traces of the entrance). (e) Hypha tunneled into muscovite, which shows possible penetration points (black circles). The white edge (inset) of the substrate clearly shows one of the penetration sites (round opening).

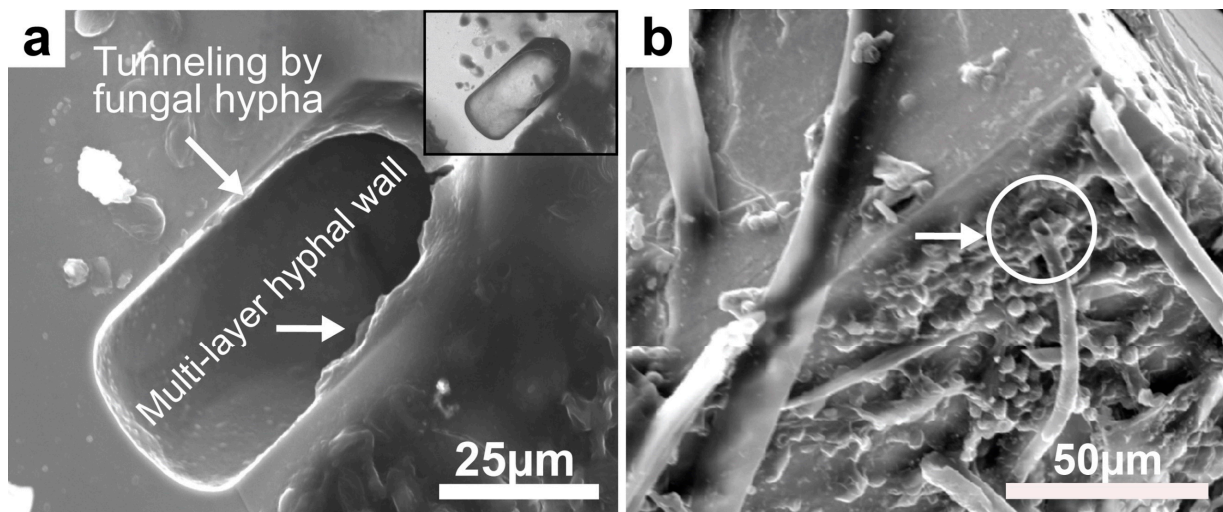


Figure 23. (a) SEM image of hypha tunneling into galena. The broken hollow hypha appears to have perforated into a galena crystal. The hypha clearly displays a multilayer wall (an indication of an organic wall), and the backscattered SEM image (inset) shows the wall in black, also an indication of its organic material. (b) Rigid and hollow hyphae are also found here. The broken end of the hypha (white arrow and encircled hyphal end) shows a hollow “tube” of the hypha which normally should be collapsed, but the acquired rigidity prevented it. The rigidity is attributed to the mineral encrustation on the hyphae and possible intracellular uptake of metals.

Figure 23a shows a single finding of a fungal hypha that had penetrated a galena crystal. The hypha partially displays a quasi-cross-sectional view of the multilayer wall of a hypha, while the backscattered SEM insert displays a black colored hyphal wall. In Figure 23b, an entire single rigid and tube-formed hypha is visible, which clearly displays the hyphal wall and the open and empty tubing. These hyphal manifestations (tunneling and tube rigidity) may suggest a strong bioleaching of substrate elements into, or their adsorption onto, the hyphal wall, thus creating mineralized hyphae, similar to what would be expected during a fossilization process; on the long hyphae in Figure 23b, visible mineral precipitations are present.

Pitting. The fungi produced elaborate pitting features, especially on bauxite. Some features characterize the incipient weathering stages, including decolorization of the weathered zone compared to the surroundings, as well as the initiation of quasi-circular/oval pits (Figure 24a,b). Once formed, fungi colonize the pits, and soon thereafter, a dense fungal network (black-dark gray color) preferentially surrounds the incipient pit contour (Figure 24c).

On the surfaces of the incipient pit authigenic minerals, likely metal oxalates produced by fungal interaction with the original mineral substrate develop (Figure 24d). The hyphae within this affected area usually show mineral encrustation on their surfaces. At an advanced stage of pitting, the bauxite surface is marked by clear pitting displaying well-developed 3D circular/oval forms, visible inner walls, depth, and variable diameters (Figure 25a,b). The most common feature is the circular/oval shape of the pits, which suggests selective fungal attacks on certain points of weakness or of specific compositions [5].

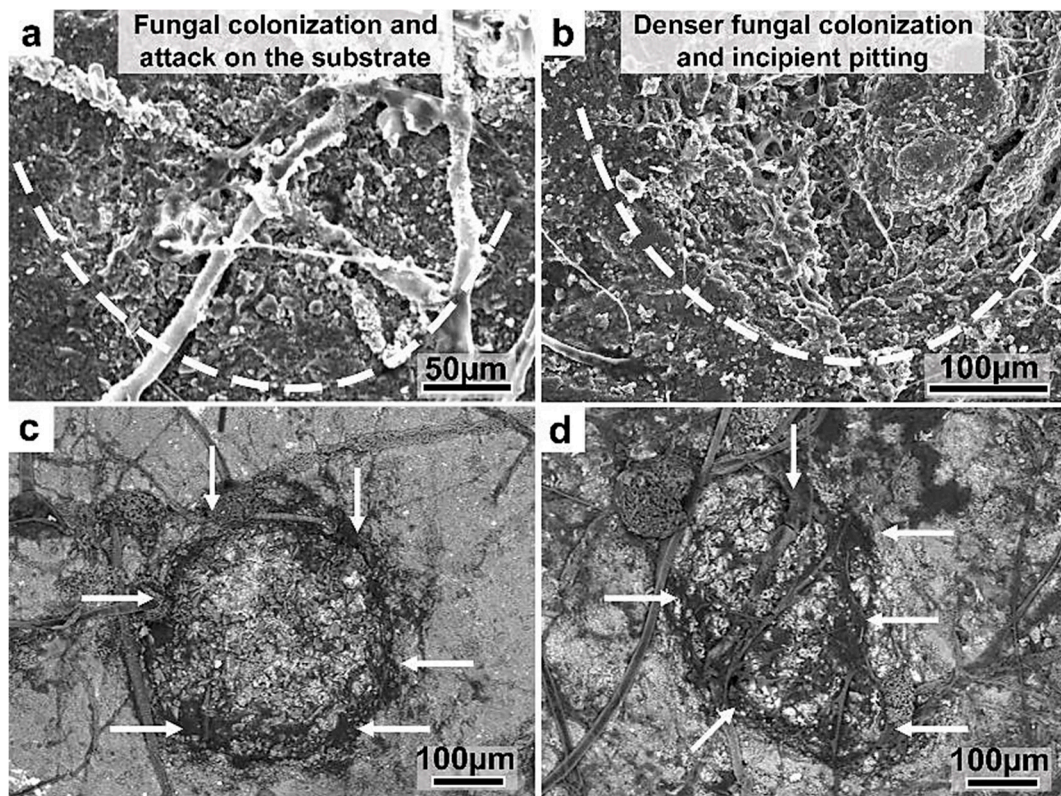


Figure 24. SEM micrographs of the fungal colonization of bauxite and the development of incipient pitting. (a) The fungi colonize and attack certain zones (area encircled by the dotted line) on bauxite, which produces de-coloration and fragmentation of the substrate. (b) A circular and deeper shape develops following the aggressive colonization, fragmentation, and dissolution of the substrate. (c,d) These backscattered images clearly show the denser fungal colonization (arrows, black-dark gray material) surrounding the attacked zones.

Once established, a fungal hyphae network develops that is interwoven well with the pit's inner walls and bottom (Figure 25c,d). Sometimes, these fungal hyphae actually form a circular "lining" to the inner walls. Authigenic Ca-oxalates (probably weddellite and whewellite) also encrust the fungal hyphae and line the inner walls of the pit (Figure 25e). Furthermore, a complex colonization pattern develops within the pits that involves real fungal hyphae invasion of the pit walls and deep penetration of the mineral matrix, which results into micro-fragmentation of the pit's wall by both mechanical dislocation and chemical dissolution in addition to the formation of biominerals such as, e.g., Mg-/Ca-oxalates, as well as the concentration of bioleached metals. Moreover, the dense fungal mass colonizing the newly formed pits (Figure 25c,d,f) and strongly interweaving with the pit's wall appears to cover the mineral's surface. Here, a whitish material is accumulated within the two fungal masses that contain high concentrations of fungally bioleached Fe.

In addition to bauxite, pitting was also evident in plagioclase. In the case of the former (Figure 26), a 3D image of a plagioclase chip displays two levels of bioweathering: dissolution of the upright surface (white and densely colonized by fungi) and pronounced pitting on the horizontal surface. The pits are typically round and form clusters with sizes ranging between 2 and 5 µm. Some pits are also visible on the upright surface.

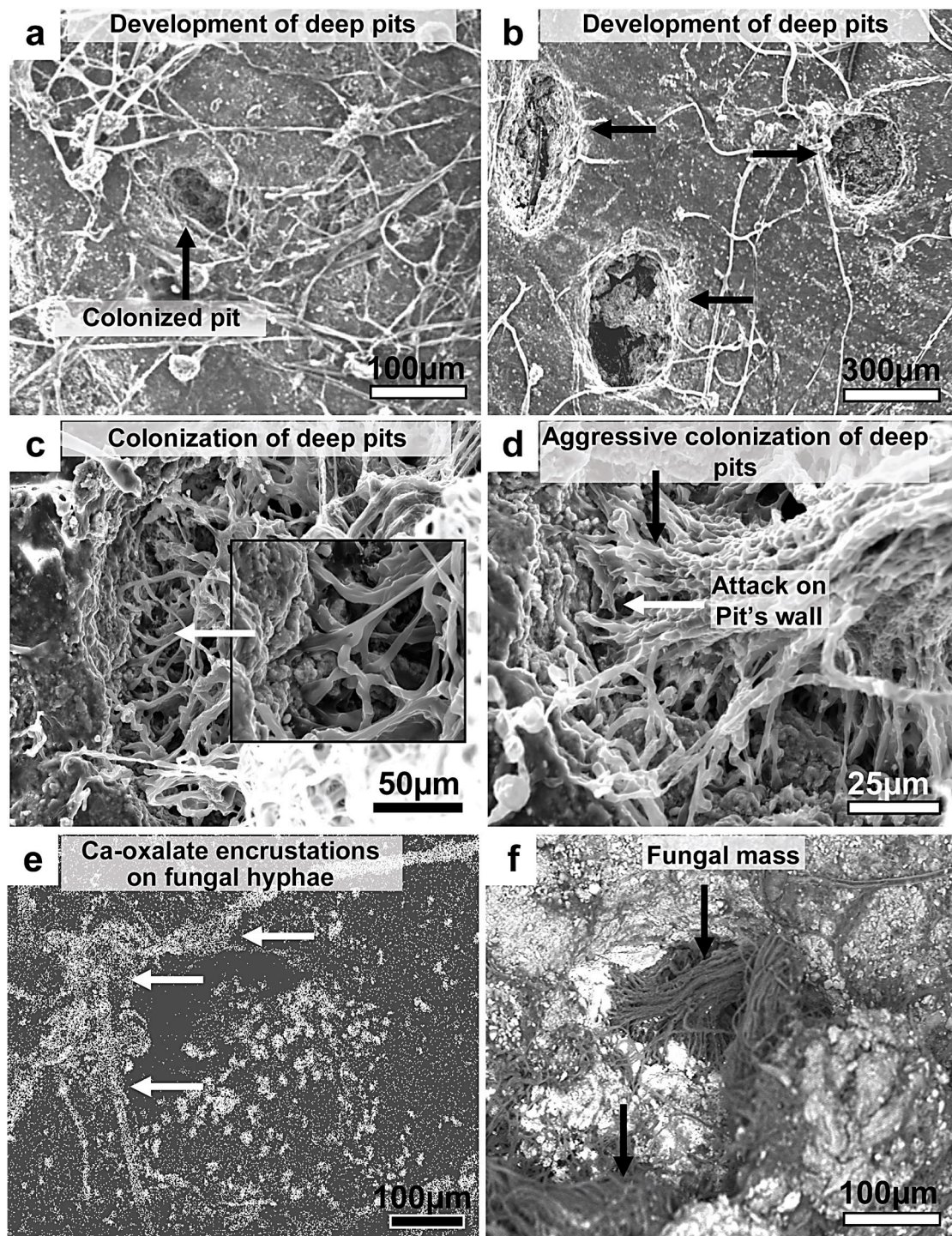


Figure 25. SEM micrographs showing the advanced pitting of bauxite. (a,b) The formation of deep oval-circular pits on bauxite, which subsequently became densely colonized by fungi. (c,d) The pit's inner walls are typically attacked by colonizing hyphae, creating an interwoven network of fungal mass lining the walls. The walls are usually degraded and fragmented. Authigenic minerals are deposited (Ca-oxalates: arrows in (e)), and the elements from the substrate are bioleached and concentrated in the fungal surroundings (arrows in (d)). (e,f) Ca SEM X-ray mapping and SEM backscattered images, respectively.

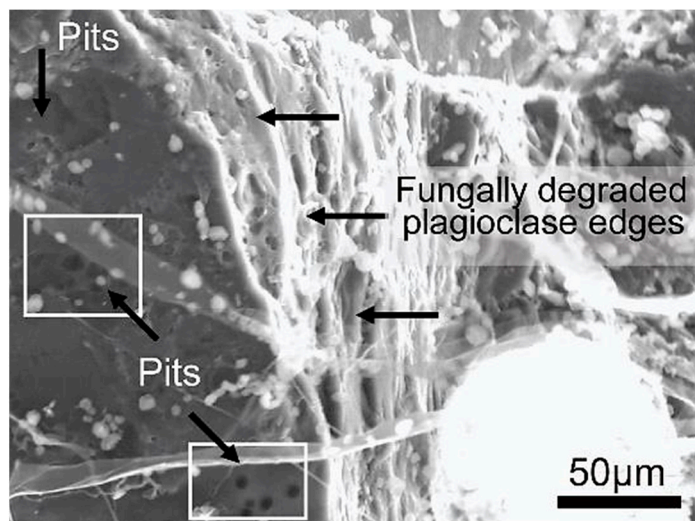


Figure 26. SEM image of a plagioclase crystal displaying round pits on its surface and degraded bio-weathered edges formed by the fungal interaction.

3.2.3. Authigenic Biomineral Formation

M-oxalates, gibbsite, and clays. As discussed earlier, certain biominerals are characteristic of fungal interactions with some substrata, e.g., limestone and dolomite. The interaction with these substrata almost invariably produces biominerals such as weddellite, whewellite, and glushinskite. Another biomineral that also formed under the conditions of this biological environment is struvite; this mineral was found occurring more on an Mg-rich substrata (biotite, muscovite, and plagioclase). The organic growth medium supplied the P. In all of the above cases, Ca and Mg were mobilized by fungi from the substrata by dissolution or direct uptake and then precipitated as authigenic biominerals on the initial mineral surfaces as encrustations on the fungal hyphae or as crystal aggregates within the fungal biomass.

When the substrata had multiple metal compositions (e.g., biotite, muscovite, and plagioclase), more elements were leached as biominerals that contained K, Ca, Mg, Al, Si, P, and Fe. Although the identity of these biominerals was not determined, their presence was clearly verified by the SEM-EDX analyses and images. It is suggested here, based on previous experience with Raman and XRD analyses, that these newly formed minerals partly contained complex oxalates, but taking into consideration the ease with which phyllosilicates are biomineralized in nature [33], these newly formed minerals (produced through a fungally induced bioweathering process) can plausibly be clay minerals, e.g., vermiculite, kaolinite, smectite, amesite, and iron oxyhydrates [34,35]. To further consider this latter possibility, we looked into one important aspect of these weathering products, i.e., the association of the prismatic lath-like, brush-like, and sheaf-like crystals with the biotite substrate. The morphology of these crystals is identical to biotite weathering into kaolinite or iron-oxyhydrates [35,36]. We have already stated (Section 3.1) that these crystals are secondary minerals precipitated from elements bioleached from the biotite substrate.

The importance of this finding is the possibility of the experimental reproduction of weathering features of biotite similar to those in nature. Our previous experimental work [25] already presented these results, but a later study [37,38] with biotite and the fungus *Suillus tomentosus* reported similar mobilization of the major elements K, Al, Mg, Si, and Fe but concluded that their experiment produced no major weathering changes to the biotite substrate.

The strong bioweathering of the biotite substrate that we reported here was caused by the direct “dry” contact between the growing fungi and the biotite substrate. To further corroborate these findings, we refer to the case of possible gibbsite $\text{Al}(\text{OH}_3)$ formation, as evidenced by the SEM-EDX chemical composition (Figure 8). Severely weathered biotite is

known to produce gibbsite [39,40]. The crystal's morphology and chemical composition and the single Al-leached mineral "gibbsite" point to a biotite bioweathering process that resembles the natural weathering of biotite under acidified conditions.

Gypsum. This is an intriguing case of authigenic mineral formation that involves the deposition of radially arranged crystal aggregates (Figure 27a) on the manganite surface. The EDX analysis showed an element composition of Ca, S, and O (Figure 27b,c) and, coupled with morphology, suggested probable gypsum. Interestingly, neither Ca nor S comprised the Mn-oxide substrate. The presence of this secondary mineral is related to the fungal material, because its position is either within or overlying the fungal organic matter biomass that colonized the manganite surface, thereby suggesting its secondary formation. Nonetheless, the source of Ca and S poses a question. In our experimental work, Ca was invariably present and associated with the fungal hyphae as encrustations or free crystals of Ca-oxalates, even when Ca was not present in the mineral substrate. Figure 27d and the Ca X-ray map inset show extensive formation of Ca-oxalates as encrustations on the fungal hyphae, as well as unattached prismatic bipyramidal crystals that litter the substrate. In this case, the single source from which Ca can be sourced is the organic growth medium. Although lacking analytical data, we similarly argue that the presence of S in the authigenic minerals is derived from the growth media.

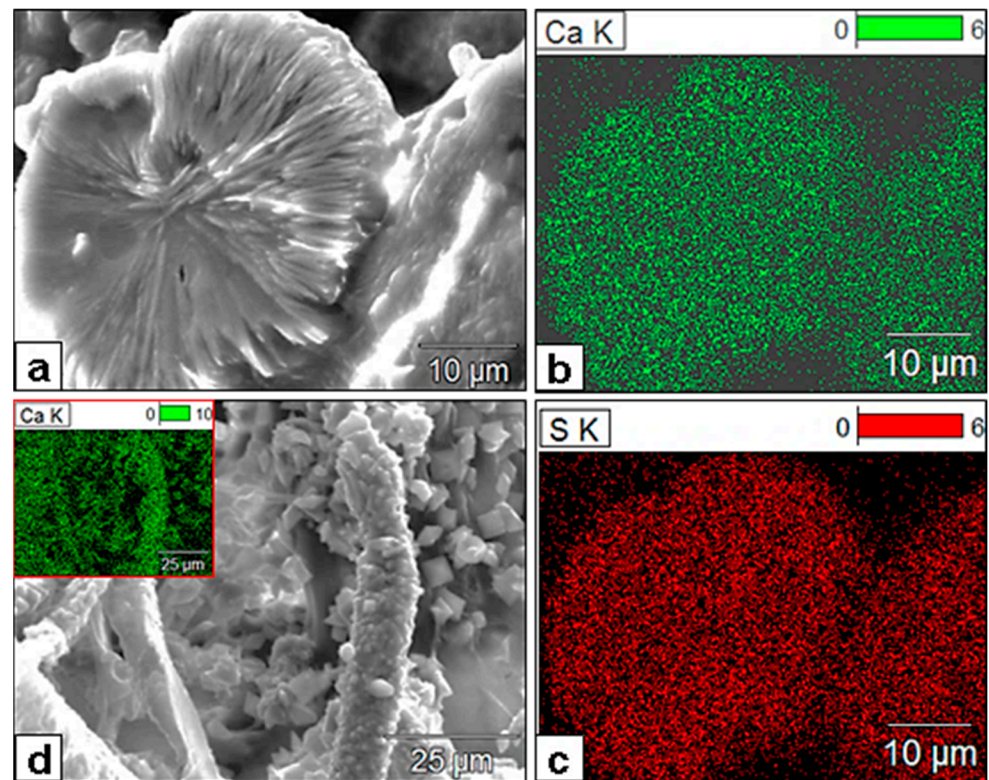


Figure 27. SEM and X-ray mapping micrographs of Ca (green) and S (red) of newly formed minerals. (a) A discock of radially arranged crystal aggregates comprising Ca, S, and O and presumed gypsum. (b,c) XR maps of the same discock, revealing the Ca and S composition of the crystal aggregates, which also extends to the composition of the much finer crystal aggregates embedded in the EPS material to the right. (d) Dense authigenic mineral formation as hyphal encrustations and free crystals that litter the background. The typical prismatic bipyramidal crystals are Ca-oxalates. The inset XR map shows their Ca composition.

The formation of gypsum on monuments, stone buildings, and concrete has been frequently attributed to the microbial interaction with the mineral substrate leading to its deterioration [41]. However, gypsum morphology similar to our experiment was reported by [42] in their study on limestone samples exposed to outdoor fungal colonization and

interaction. They found extensive gypsum formation of round-discoid aggregates and considered the polluted air as the main source of S, while Ca was supplied by the substrate.

4. Discussion

4.1. Three-Dimensional Colonization, Thigmotropism, and Metallophagus Behavior

To date, fungal colonization of mineral surfaces is generally discussed in the literature as a 2D process that involves biochemical and biomechanical processes leading to mineral degradation and weathering. However, this view overlooks the ability of fungi to penetrate into mineral substrata through the thigmotropic sensing of mineral surfaces and their ulterior colonization. The pattern mode of that colonization has not been reported previously, especially when the minerals have well-developed crystal habits with multiple exposed faces. For example, experimental studies that involve fungi as plant pathogens have shown that fungi recognize the stomatal apertures by using topographic “contact sensing” [43–46]. Thigmotropism, since it was originally observed by [47] and up to the current literature, is restricted to pathogenic fungi attacking plants or human cells such as *Candida albicans*, although that fungal growth is known to occur on a two-dimensional or three-dimensional matrix (see, e.g., [48]) similar to mineral surfaces and arrangement, yet concepts relating that type of growth to thigmotropism and contact sense were not developed for minerals. Actually, as it will be further discussed below, that pathogenic behavior of certain fungi with plants and human cells can be extrapolated to fungi colonizing mineral surfaces in exceptional 3D patterns on a microscale where processes of dissolution and alteration and the absorbance of elements from those substrates convey the concept of mineral pathogenesis that is caused by fungal colonization and metallophagus behavior.

In this study, we combined the use of 2D thin sections to mineral surfaces (e.g., dolomite and calcite) that only provided a 2D perspective of the alteration processes with the analysis of 3D spatial topography when using large mineral crystals with relatively high angles and sharp intersections (e.g., galena, chromite, manganite, and malachite) in “dry contact” colonization conditions (the growing fungi were at a distance from the minerals, and colonization was achieved as a result of the exploratory search by fungi). In the latter case, the fungi showed a marked thigmotropic “contact-sensing” behavior towards the exposed mineral substrates. In our study, the results show that the fungal behavior is similar to that of plants’ fungal pathogens in that there is a 3D topographic sensing leading to the colonization of all exposed mineral faces.

(1) Close attachment (adherence) [49,50] is necessary for sensing the topography (recall Figures 1a–e and 2a–c). The fungal hyphae upon colonization of a new surface display an evident angle of approach (contact angle) to the surface before changing growth orientation or direction relative to the new colonized surface. This has not been described before in fungal species colonizing mineral surfaces nor has it been implied, but it has been well demonstrated in experimental studies with fungal species acting as plant pathogens, e.g., [45,46]. In our examples (Figure 2a–c), at the angle of contact with a mineral surface, the hyphae develop an attachment anchor, evidently with a mucilage substance, showing side threads (Figure 2b) that ensure the adherence of the hypha to the mineral surface before the change of growth direction as the fungi attempt to colonize the other remaining exposed surfaces. Close adhesion is required for sensing of the topography.

(2) The exploratory nature of fungal hyphae and their selective colonization of different minerals with different surface topologies (the most important being the distance separating them from the growth centers on the base of the Petri dishes) further suggests “contact sensing” and thigmotropism, as observed in the previous section. The contact sensing and mineral surface recognition noted in this case are highlighted by the preferential selection of the lamellae edges over the plane surfaces. Physically, these edges represent weaker structural points as compared to the more compact planar surfaces for fungal attack and colonization. Furthermore, pathogenic fungi (e.g., *Uromyces appendicalatus*, *Puccinia hordei*, or *Candida Albicans*) at contact with an elevated ridge and depending on the elevation and angle of approach, develop appressoria as an anchoring device. This has not been

reported for fungi attacking minerals. But in a close study of Figure 2b (and less evident in Figure 2c), we observe a flattening and enlargement of the fungal hyphae exactly at the crossing of intersection line of the exposed mineral faces, similar to appressoria formation at ridges on experimental polystyrene microtopography wafers [43–45]. The similarity suggests (though cautiously) a probable formation of appressoria even by fungi that attack minerals. This probability is further strengthened by the fact that the reorientation of the apically growing fungi (Figure 2a,c) occurs almost at 90° to the face lineaments, i.e., the crystal's planes of intersection. We have no concrete explanation for this behavior so far in what concerns minerals, but the growth of germ tubes in cereal rust fungi *Puccinia graminis tritici* and *Puccinia hordei* orientate at right angles to a series of equally spaced ridges and grooves [43], an exemplification of the leaf stomata searching by fungi and a prelude to plant infection.

The geometrical positioning of the experimental samples: vertical–horizontal, suspended above the growth medium, and random arrangement of large mineral crystals exposing mineral surfaces at various angles, all situated at reasonable distance from the growing fungi, was important in concluding that the colonization of the minerals was actually driven by thigmotropic as well as metalophagus behavior. This is most strongly demonstrated by the selective behavior of colonizing biotite and muscovite edges compared to the rest of the exposed surface. In the same line of discussion, Figure 1e shows a galena crystal entirely engulfed by colonizing fungi, while an adjacent much smaller crystal is practically noncolonized. This also suggests colonization selectivity, where possibly the crystal size plays a role.

(3) Besides showing an exploratory behavior, the fungi may also be displaying a metalophagus response during colonization, as briefly discussed before. The notion of “rock-eating fungi” has been already introduced into specialized literature [51], but since, it has been repeatedly [52] used to refer to the interaction of ectomycorrhizal fungi with podzol mineral (Al, Ca, Mg, and P) dissolution and tunneling. Our experimental results point towards a different interpretation of fungal interaction with minerals, i.e., a metalophagus behavior derived from the observation of the 3D colonization pattern, thigmotropism, and hyphae–mineral contact angle. This interpretation proposes that fungi with their mycelial structure collectively can act as a unit, breaking down and digesting certain mineral substrates. Taking into consideration that few minerals comprise toxic metals (e.g., Pb in galena, Cr in chromite, Al in bauxite, and Cu in malachite), this could be seen as a defensive process through metal immobilization, sequestration leading to the biomineralization of new biogenic minerals, besides the main process of nutrient extraction by dissolution.

4.2. Bioweathering

All the minerals used in the experimental work showed variable degrees of bioweathering (fragmentation, dissolution, tunneling, pitting, exfoliation, and bioleaching) related directly to the colonizing fungal activity. By far, the most visible effects of this activity were observed on the carbonate substrata, which were called diagenetic rather than bioweathering because of their resemblance to diagenesis in sediments [5].

Biomechanical/biochemical weathering. The invasive action of fungal hyphae into grain boundaries, cleavages, cracks, and fractures produces enough mechanical pressure to dislocate grain or mineral laminations and leads to their fragmentation or exfoliation [4,53,54]. This is facilitated by fungal thigmotropism, where the direction of fungal growth is influenced by grooves, ridges, and pores in the mineral substrate [1,2], and we can certainly add here, by the phagocytic (e.g., Figure 1) and mineral composition (Figures 24 and 25) where fungi have targeted certain areas on the bauxite substrate and where the pits developed. Once a pit is developed, fungi continue their mechanical weathering effect through both further dissolution and dislocation of the grains, and the process will continue as long as colonization continues. In this regard, it is not possible to separate the mechanical effect exerted by the turgor pressure inside the fungal hyphae from the biochemical one, which is produced by the organic acid exudates. Biotite (Figure 19d),

the biomechanical force of the intralayer intrusive hyphae. The edges clearly show the marks of dissolution. A more interesting case is demonstrated in Figure 28b, because it shows a typical weathering reaction of biotite by expansion and buckling associated with secondary mineral deposition at the margins. The swollen, buckled, and broken middle part of the biotite is comparable to natural weathering of biotite reported in several studies [36,55]. This is the first report on obtaining experimental bioweathering results similar to natural ones.

The felsic minerals exhibit more resistance to weathering due to their extensively cross-linked structure [56]. In an acidified environment, the protons adsorb onto mineral surfaces and induce a rearrangement of the charge in the silicate lattice and, hence, hydrolysis of the surface Al-O-Si bonds. Microbial organic acids can increase the rates of feldspar dissolution by orders of magnitude [13]. Compared to biotite, muscovite has shown less frequency in bioweathering features, although the main aspects of bioweathering were observed, such as lamella edges dissolution, channeling, exfoliation, and fragmentation (Figures 10, 11, 19c,d and 21d). The bioweathering was also associated with the secondary mineral formation (Figure 21d).

However, the removal of Si from substrates and its incorporation into the biologically mediated formation of minerals, such as is in the present case, is only reported in plants and certain aquatic organisms such as diatoms and sponges where SiO₂ is incorporated into the plant cell wall for enhancing the mechanical strengths, as well as biotic and abiotic stress [57]. Silicon uptake by organisms is in the form of orthosilicic acid (Si[OH]₄), which is subsequently polymerized into insoluble silica through the biosilicification process [58]. Silicic acid is essential in promoting fungal growth [59]. In the present work, the Si availability in the fungal growth environment is possibly driven by the bioleaching of Si from Si-rich substrates, leading to silicic acid formation. Here, it is difficult to specify whether the formed silicic acid complexed with other elements to form new minerals (Figure 7) or if it was chelated organically into fungi (Figure 6).

Tunneling. During the course of our experiment, real tunneling (including the channels) by the fungi was only observed on the silicate minerals biotite and muscovite. In the literature, the most evident cases of tunneling have been reported for European podzol soils [28,51] in podzol feldspars in North Sweden. Although it is accepted that ectomycorrhizal fungi (EMF) are involved in the tunneling of feldspars [29], such fungal involvement has been strongly criticized [60]. But bioweathering tunneling that has been attributed to undefined microbial activity is not scarce in the literature [61,62], especially when associated with iron-magnesium silicate minerals. For instance, [61] reported the finding of microbial tunnels in olivine and pyroxene of oceanic basalt and Oregon dunite and concluded that microorganisms produce these micro-tunnels. Hence, it may be inevitable not to suggest that microbial tunneling is likely to be associated (if not restricted) with a variety of silicate minerals. In the present experimental results, only biotite and muscovite were subject to tunneling by the fungi with reasonable frequency. The other minerals showed other bioweathering signatures but not tunneling (apart from the single case of galena). The micro-tunnels reported by [62] on oceanic basalt samples can be easily compared to the ones produced by fungi, both morphologically and the manner of their points of entrance (Figure 22e). It is also worth mentioning that, while the process of feldspars tunneling by EMF is considered to have taken many thousands of years [28], our results show that fungi are practically capable of producing these tunnels in biotite and muscovite within weeks of time, and additionally, this tunneling into silicate minerals is not restricted to ectomycorrhizal fungi but is shared by other species such as *Aspergillus flavus* and *Rhizopus oryzae*.

On the other hand, fungal hyphae in cross-sections displaying circular walls and penetrating a carbonate substratum have been shown in other studies [63]. Fungal tunneling in phyllosilicates, feldspars, and carbonates has been linked to the presence of Ca, P, K, and Al in these minerals and their role in fungal growth and nutrient search activities. But in galena, due to its Pb-S composition, this could raise different questions, since no Pb or S

has been reported to play a role in the above activities. Apart from specific interactions (exfoliation, pitting, and solubilization) between fungi and galena crystals, demonstrated in this and in other studies [64,65], the fungal tunneling of galena needs further consideration.

5. Conclusions

Within 10 days of the 12-week experiment of exposing various mineral surfaces to the air, thick fungal mats colonized the surfaces of every mineral substrate, irrespective of chemistry, mineralogy, and surface configuration. In all the cases, the fungal hyphae showed a marked ability to attach to a mineral surface, establish an anchorage, and perform multiple growth direction changes in response to the crystal face geometry reaching approximately 90° angles. Mineral surface thigmotropism was established on a microscale, where the fungi clearly recognized the microtopography, surfaces, and angles to direct the hyphal growth direction. It is also suggested that the size of the exposed crystals played a certain role in the 3D colonization. The horizontal and vertical positioning of biotite and muscovite lamellae revealed a selective thigmotropic preference to colonize and invade the edges even at a distance from growth center, and in some instances, the fungi showed metalophagus behavior in that the fungi responded defensively to some trace metal component in the substrate. Tunneling into minerals (biotite, muscovite, and galena) by hyphae was also important and showed an interaction that has, so far, only been reported for ectomycorrhizal fungi. Collectively, pitting, fragmentation, exfoliation, bioleaching, and authigenic biomineral formation confirm that colonizing fungi effectively contribute to mineral bioweathering.

Author Contributions: Conceptualization, K.K.; methodology, K.K.; software, K.K.; validation, K.K. and A.P.; formal analysis, K.K.; investigation, K.K.; resources, K.K. and A.P.; data curation, K.K.; writing—original draft preparation, K.K.; writing—review and editing K.K. and A.P.; visualization, K.K. and A.P.; supervision, A.P.; project administration, K.K. and A.P.; funding acquisition, A.P. All authors have read and agreed to the published version of the manuscript.

Funding: The study benefitted from research funds from the Universite Libre de Bruxelles (ULB)-Belgium.

Data Availability Statement: The data presented in this study are available in the article.

Acknowledgments: Thanks are due to the Department of Metallurgy/Vrije Universiteit Brussel, for their valuable assistance with the SEM and FE-SEM, especially to Oscar Steenhaut. We also appreciate the XRD analysis facility and assistance offered by the Department of Industrial Chemistry, Université Libre de Bruxelles, and by Tiriana Segato.

Conflicts of Interest: The authors declare no conflict of interest.

References

1. Burford, E.P.; Fomina, M.; Gadd, G.M. Fungal involvement in bioweathering and biotransformation of rocks and minerals. *Miner. Mag.* **2003**, *67*, 1127–1155. [[CrossRef](#)]
2. Burford, E.P.; Kierans, M.; Gadd, G.M. Geomycology: Fungi in mineral substrata. *Mycologist* **2003**, *17*, 98–107. [[CrossRef](#)]
3. Hoffland, E.; Kuyper, T.W.; Wallander, H.; Plassard, C.; Gorbushina, A.A.; Haselwandter, K.; Holmström, S.; Landeweert, R.; Lundström, U.S.; Rosling, A.; et al. The role of fungi in weathering. *Front. Ecol. Environ.* **2004**, *2*, 258–264. [[CrossRef](#)]
4. Gadd, G.M. Geomycology: Biogeochemical transformations of rocks, minerals, metals and radionuclides by fungi, bioweathering and bioremediation. *Mycol. Res.* **2007**, *111*, 3–49. [[CrossRef](#)] [[PubMed](#)]
5. Kolo, K.; Keppens, E.; Pr at, A.; Claeys, P. Experimental observations on fungal diagenesis of carbonate substrata. *J. Geophys. Res.* **2007**, *112*, G01007. [[CrossRef](#)]
6. Chen, J.; Blume, H.-P.; Beyer, L. Weathering of rocks induced by lichen colonization—A review. *CATENA* **2000**, *39*, 121–146. [[CrossRef](#)]
7. Landeweert, R.; Veenman, C.; Kuyper, T.W.; Fritze, H.; Wernars, K.; Smit, E. Quantification of ectomycorrhizal mycelium in soil by real-time PCR compared to conventional quantification techniques. *FEMS Microbiol. Ecol.* **2003**, *45*, 283–292. [[CrossRef](#)] [[PubMed](#)]
8. Hendricks, J.J.; Mitchell, R.J.; Kuehn, K.A.; Pecot, S.D.; Sims, S.E. Measuring external mycelia production of ectomycorrhizal fungi in the field: The soil matrix matters. *New Phytol.* **2006**, *171*, 179–186. [[CrossRef](#)]
9. Golubic, S.; Gudrun, R.; Le Campion-Alsumard, T. Endolithic fungi in marine ecosystems. *Trends Microbiol.* **2005**, *13*, 229–235. [[CrossRef](#)]

10. Sterflinger, K. Fungi as Geologic Agents. *Geomicrobiol. J.* **2000**, *17*, 97–124. [[CrossRef](#)]
11. Warscheid, T.; Braams, J. Biodeterioration of stone: A review. *Int. Biodeterior. Biodegrad.* **2000**, *46*, 343–368. [[CrossRef](#)]
12. Rios, A.; Ascaso, C. Contributions of in situ microscopy to the current understanding of stone bioteriation. *Int. Microbiol.* **2005**, *8*, 181–188. [[PubMed](#)]
13. Konhauser, K. *Introduction to Geomicrobiology*; Blackwell Publishing: Hoboken, NJ, USA, 2007.
14. Taylor, N.; Osborn, M. The importance of fungi in shaping the paleoecosystem. *Rev. Palaeobot. Palynol.* **1996**, *90*, 249–262. [[CrossRef](#)]
15. Brundrett, M.C. Coevolution of roots and mycorrhizas of land plants. *New Phytol.* **2002**, *154*, 275–304. [[CrossRef](#)] [[PubMed](#)]
16. Gadd, G.M. The Geomycology of Elemental Cycling and Transformations in the Environment. *Microbiol. Spectr.* **2017**, *5*. [[CrossRef](#)]
17. Gadd, G.M. Fungal production of citric and oxalic acid: Importance in metal speciation, physiology and biogeochemical processes. *Adv. Microb. Physiol.* **1999**, *41*, 47–92. [[PubMed](#)]
18. Sayer, J.A.; Gadd, G.M. Solubilization and transformation of insoluble inorganic metal compounds to insoluble metal oxalates by *Aspergillus niger*. *Mycol. Res.* **1997**, *101*, 653–661. [[CrossRef](#)]
19. Gadd, G.M. Fungal influence on mineral dissolution and metal mobility: Mechanisms and biogeochemical relevance. In Proceedings of the 12th Annual Goldschmidt Conference, Davos, Switzerland, 18–23 August 2002. Abstracts A257.
20. Gadd, G.M.; Burford, E.P.; Fomina, M.; Harper, F.A.; Jacobs, H. Fungal influence on metal mobility: Mechanisms and relevance to environment and biotechnology. In Proceedings of the 7th International Mycological Congress, Oslo, Norway, 11–17 August 2002. Abstract No. 328.
21. Lee, M.R.; Parsons, I. Biomechanical and biochemical weathering of lichen-encrusted granite: Textural controls on organic-mineral interactions and deposition of silica-rich layers. *Chem. Geol.* **1999**, *161*, 385–397. [[CrossRef](#)]
22. Kolo, K.; Claeys, P. In vitro formation of Ca-oxalates and the mineral glushinskite by fungal interaction with carbonate substrata and seawater. *Biogeosciences* **2005**, *2*, 451–497. [[CrossRef](#)]
23. Russ, J.; Palma, R.L.; Loyd, D.H.; Boutton, T.W.; Coy, M. Origin of the whewellite-rich rock crust in the lower region of southwest Texas and its significance to paleoclimatic reconstructions. *Quat. Res.* **1996**, *46*, 27–36. [[CrossRef](#)]
24. Verrecchia, E.P. Fungi and sediments. In *Microbial Sediments*; Riding, R.E., Awramik, S.M., Eds.; Springer: New York, NY, USA, 2000; pp. 68–75.
25. Arocena, J.M.; Zhu, L.P.; Hall, K. Mineral accumulations induced by biological activity on granitic rocks in Qindhai Plateau, China. *Earth Surf. Process. Landf.* **2003**, *28*, 1429–1437. [[CrossRef](#)]
26. Fraç, M.; Hannula, S.E.; Beřka, M.; Jędryczka, M. Fungal biodiversity and their role in soil health. *Front. Microbiol.* **2018**, *9*, 707. [[CrossRef](#)]
27. Bowen, A.D.; Davidson, F.A.; Keatch, R.; Gadd, G.M. Induction of contour sensing in *Aspergillus niger* by stress and its relevance to fungal growth mechanics and hyphal tip structure. *Fungal Genet. Biol.* **2007**, *44*, 484–491. [[CrossRef](#)] [[PubMed](#)]
28. Hoffland, E.; Giesler, R.; Jongmans, T.; van Breemen, N. Increasing feldspar tunneling by fungi across a north Sweden podzol chronosequence. *Ecosystems* **2002**, *5*, 11–22. [[CrossRef](#)]
29. Smits, M.M.; Hoffland, E.; Jongmans, A.G.; van Breemen, N. Contribution of mineral tunneling to total feldspar weathering. *Geoderma* **2005**, *125*, 59–69. [[CrossRef](#)]
30. Moore, D. Gravid responses in fungi. *Adv. Space Res.* **1996**, *17*, 73–82. [[CrossRef](#)] [[PubMed](#)]
31. Kern, V.D. Gravitropism of Basidiomycetes fungi—On Earth and in microgravity. *Adv. Space Res.* **1999**, *24*, 697–706. [[CrossRef](#)]
32. Hock, B.; Häder, D.P. Gravid responses in fungi and slime molds. *Signal Transduct.* **2006**, *6*, 443–448. [[CrossRef](#)]
33. Konhauser, K.O.; Fisher, Q.J.; Fyfe, W.S.; Longstaffe, F.J.; Powell, M.A. Authigenic mineralization and detrital clay binding by freshwater biofilms: The Brahmani River, India. *Geomicrobiol. J.* **1998**, *15*, 209–222. [[CrossRef](#)]
34. Grant, W.H. Chemical weathering of biotite–plagioclase gneiss. *Clays Clay Miner.* **1963**, *12*, 455–463. [[CrossRef](#)]
35. Bisdom, E.B.A.; Stoops, G.; Delvigne, J.; Curmi, P.; He, J.A. Micromorphology of Weathering Biotite and Its Secondary Products. *Pedologie* **1982**, *2*, 225–252.
36. Wierzbos, J.; Ascaso, C. Morphological and chemical features of bioweathered granitic biotite induced by lichen activity. *Clays Clay Miner.* **1996**, *44*, 652–657. [[CrossRef](#)]
37. Balogh-Brunstad, Z.; Keller, C.; Gill, R.; Bormann, B.; Li, C. The effect of bacteria and fungi on chemical weathering and chemical denudation fluxes in pine growth experiments. *Biogeochemistry* **2008**, *88*, 153–167. [[CrossRef](#)]
38. Balogh-Brunstad, Z.; Keller, C.; Dickinson, J.; Stevens, F.; Li, C.Y.; Bormann, T. Biotite weathering and nutrient uptake by ectomycorrhizal fungus, *Suillus tomentosus*, in liquid-culture experiments. *Geochim. Et Cosmochim. Acta* **2008**, *72*, 2601–2618. [[CrossRef](#)]
39. Jolicoeur, S.; Ildefonse, P.; Bouchard, M. Kaolinite and Gibbsite Weathering of Biotite within Saproilites and Soils of Central Virginia. *Soil Sci. Soc. Am. J.* **2000**, *64*, 1118–1129. [[CrossRef](#)]
40. Herrmann, L.; Anongrak, N.; Zarei, M.; Schuler, U.; Spohrer, K. Factors and processes of gibbsite formation in Northern Thailand. *CATENA* **2007**, *71*, 279–291. [[CrossRef](#)]
41. Flores, M.; Lorenzo, J.; Gómez-Alarcón, G. Algae and bacteria on historic monuments at Alcalá de Henares, Spain. *Int. Biodeterior. Biodegrad.* **1997**, *40*, 241–246. [[CrossRef](#)]
42. Moroni, B.; Pitzurra, L. Biodegradation of atmospheric pollutants by fungi: A crucial point in the corrosion of carbonate building stone. *Int. Biodeterior. Biodegrad.* **2008**, *62*, 391–396. [[CrossRef](#)]

43. Read, N.D.; Kellock, L.J.; Collins, T.J.; Gundlach, A.M. Role of topography sensing for infection-structure differentiation in cereal rust fungi. *Planta* **1997**, *202*, 163–170. [[CrossRef](#)]
44. Collins, T.J.; Read, N.D. Appressorium induction by topographical signals in six cereal rusts. *Physiol. Mol. Plant Pathol.* **1997**, *51*, 169–179. [[CrossRef](#)]
45. Allen, E.A.; Hazen, B.E.; Hoch, H.C.; Kwon, Y.; Leinhos, G.M.E. Appressorium formation in response to topographical signals by 27 rust species. *Phytopathology* **1991**, *81*, 323–331. [[CrossRef](#)]
46. Gow, N.A.R. New angles in mycology: Studies in directional growth and directional motility. *Mycol. Res.* **2004**, *108*, 5–13. [[CrossRef](#)] [[PubMed](#)]
47. Drechsler, C. Some hyphomycetes that prey on free-living terricolous nematodes. *Mycologia* **1937**, *29*, 447–552. [[CrossRef](#)]
48. Almeida, M.C.; Brand, A.C. Thigmo Responses: The Fungal Sense of Touch. *Microbiol. Spectr.* **2017**, *5*. [[CrossRef](#)] [[PubMed](#)]
49. Jaffe, M.J.; Leopold, A.C.; Staples, R.C. Thigmo responses in plants and fungi. *Am. J. Bot.* **2002**, *89*, 375–382. [[CrossRef](#)] [[PubMed](#)]
50. Mendgen, K.; Hahn, M.; Deising, H. Morphogenesis and Mechanisms of Penetration by Plant Pathogenic Fungi. *Annu. Rev. Phytopathol.* **1996**, *34*, 367–386. [[CrossRef](#)] [[PubMed](#)]
51. Jongmans, A.G.; van Breemen, N.; Lundstrom, U.; van Hees, P.A.W.; Finlay, R.D.; Srinivasan, M.; Unestam, T.; Giesler, R.; Melkerud, P.; Olsson, M. Rock-eating fungi. *Nature* **1997**, *389*, 682–683. [[CrossRef](#)]
52. Van Breemen, N.; Lundström, U.S.; Jongmans, A.G. Do plants drive podzolization via rock-eating mycorrhizal fungi? *Geoderma* **2000**, *94*, 163–171. [[CrossRef](#)]
53. Banfield, J.F.; Barker, W.W.; Welch, S.A.; Taunton, A. Biological impact on mineral dissolution: Application of the lichen model to understanding mineral weathering in the rhizosphere. *Proc. Natl. Acad. Sci. USA* **1999**, *96*, 3404–3411. [[CrossRef](#)]
54. Kumar, R.; Kumar, A.V. *Biodeterioration of Stone in Tropical Environments: An Overview*; The Getty Conservation Institute: Santa Monica, CA, USA, 1999.
55. Wierzchos, J.; Ascaso, C. Mineralogical transformation of bioweathered granitic biotite, studied by HRTEM; evidence for a new pathway in lichen activity. *Clays Clay Miner.* **1998**, *46*, 446–452. [[CrossRef](#)]
56. Brady, V.P.; Walther, V.J. Controls on silicate dissolution rates in neutral and basic pH solutions at 25 °C. *Geochim. Cosmochim. Acta* **1989**, *53*, 2823–2830. [[CrossRef](#)]
57. Feng, Y.; Hana, H.; Nonga, W.; Tanga, J.; Chena, X.; Lia, X.; Shib, L.; Kreslavskic, D.; Allakhverdiev, I.; Shabalaa, S.; et al. The biomineralization of silica induced stress tolerance in plants: A case study for aluminum toxicity. *Plant Signal. Behaviour.* **2023**, *18*, 2233179. [[CrossRef](#)]
58. Ikeda, T. Bacterial biosilicification: A new insight into the global silicon cycle. 2021. *Biosci. Biotechnol. Biochem.* **2021**, *85*, 1324–1331. [[CrossRef](#)]
59. Wainwright, M.; Al-Wajeeh, K.; Grayston, S.J. Effect of silicic acid and other silicon compounds on fungal growth in oligotrophic and nutrient-rich media. *Mycol. Res.* **1997**, *101*, 933–938. [[CrossRef](#)]
60. Sverdrup, H.; Hagen-Thorn, A.; Holmqvist, J.; Wallman, P.; Warfvinge, P.; Walse, C.; Alveteg, M. Biogeochemical processes and mechanisms. In *Developing Principles and Models for Sustainable Forestry in Sweden*; Sverdrup, H., Stjernquist, I., Eds.; Kluwer Academic Publishers: Dordrecht, The Netherlands, 2002.
61. Popa, R.; Nealsen, K.H.; Fisk, M.R.; Souza-Egipsy, V. Micron-size tunnels in olivines in basaltic lava. In *European Workshop on Exo/Astrobiology*, 3rd ed.; European Space Agency Special Publication 545; European Space Agency: Noordwijk, The Netherlands, 2004; pp. 77–80.
62. Fisk, M.R.; Popa, R.; Mason, O.U.; Storrie-Lombardi, M.C.; Vicenzi, E.P. Iron-Magnesium Silicate Bioweathering on Earth (and Mars?). *Astrobiology* **2006**, *6*, 48–68. [[CrossRef](#)]
63. Hoppert, M.; Flies, C.; Pohl, W.; Günzl, B.; Schneider, J. Colonization strategies of lithobiontic microorganisms on carbonate rocks. *Environ. Geol.* **2004**, *46*, 421–428. [[CrossRef](#)]
64. Sayer, J.A.; Kierans, M.; Gadd, G.M. Solubilisation of some naturally occurring metal-bearing minerals, limescale and lead phosphate by *Aspergillus niger*. *FEMS Microbiol. Lett.* **1997**, *154*, 29–35. [[CrossRef](#)] [[PubMed](#)]
65. Adeyemi, A.O.; Gadd, G.M. Fungal degradation of calcium-, lead- and silicon-bearing minerals. *BioMetals* **2005**, *18*, 269–281. [[CrossRef](#)] [[PubMed](#)]

Disclaimer/Publisher’s Note: The statements, opinions and data contained in all publications are solely those of the individual author(s) and contributor(s) and not of MDPI and/or the editor(s). MDPI and/or the editor(s) disclaim responsibility for any injury to people or property resulting from any ideas, methods, instructions or products referred to in the content.